Archives of Civil and Mechanical Engineering (2024) 24:68
https://doi.org/10.1007/s43452-024-00874-0

ORIGINAL ARTICLE

Seismic vulnerability estimation of RC structures considering empirical and numerical simulation methods

Si-Qi Li[1,2] · Ke Du[1] · Yi-Ru Li[1] · Jia-Cheng Han[1] · Peng-Fei Qin[1] · Hong-Bo Liu[1]

Received: 20 November 2023 / Revised: 4 January 2024 / Accepted: 17 January 2024 / Published online: 5 March 2024

Abstract

Empirical and probabilistic risk analysis methods can relatively accurately predict the seismic vulnerability of reinforced concrete (RC) structures. Using various intensity measures to estimate and forecast the seismic hazard of RC structures can contribute to the development of typical structural seismic resilience and vulnerability models. However, traditional empirical and analytical vulnerability studies rely more on field observation data and seismic risk algorithms and less on numerical simulation analysis for validation and optimization, resulting in limitations and fuzziness in the accuracy of the developed structural risk models. To explore the damage modes of RC frame structures under different intensities, this paper innovatively combines numerical model algorithms with empirical vulnerability methods to conduct empirical vulnerability and numerical simulation analyses on RC structures. Using probability statistics and nonlinear regression analysis methods, a prediction model for estimating the fragility of RC structures was proposed, and 858 RC structure damage samples from a typical city (Dujiangyan) during the Wenchuan earthquake in China on May 12, 2008, were used for model verification and comparative analysis. Using seismic response analysis theory, 901,530 acceleration records of the Wenchuan earthquake detected by eight actual seismic stations were selected, and nonlinear dynamic time history analysis was conducted. A four-story RC structural model was established using finite element software, and numerical simulation analysis was conducted on the model using 117,863 real earthquake acceleration data points obtained from actual monitoring stations during the Wenchuan earthquake. The acceleration time history curves and incremental dynamic analysis curves of the RC structure under different intensity measures were generated. By combining the moire algorithm and numerical simulation technology, damage stress clouds of steel bars and concrete under different intensity measures were generated, and the accuracy of the developed empirical vulnerability model was verified via numerical simulation results.

Keywords Empirical seismic vulnerability · Numerical simulation analysis · Reinforced concrete structure · Damage modal analysis · Structural failure analysis

✉ Si-Qi Li
lisiqi@hlju.edu.cn

Ke Du
duke0724@163.com

Yi-Ru Li
liyiru312@163.com

Jia-Cheng Han
17860061789@163.com

Peng-Fei Qin
qpf443028797@163.com

Hong-Bo Liu
hongboliuhlju@126.com

[1] School of Civil Engineering, Heilongjiang University, No. 74, Xuefu Road, Harbin, China

[2] Institute of Engineering Mechanics, China Earthquake Administration, Key Laboratory of Earthquake Disaster Mitigation, Ministry of Emergency Management, Heilongjiang University Key Laboratory of Earthquake Engineering and Engineering Vibration, Harbin Institute of Technology, Harbin, China

1 Introduction

Seismic vulnerability refers to the conditional probability of engineering structures reaching or exceeding a given damage state under different earthquake intensities. Seismic vulnerability can quantitatively characterize the seismic performance of structures in terms of probability. Simultaneously, the quantitative relationship between the intensity of seismic motion and the degree of structural damage can also be described from a macro perspective. Seismic vulnerability can also be understood as the overall seismic performance of a structure, which is the ability of the structure to resist seismic effects (Hu [1]). Evaluating structural vulnerability using actual seismic intensity indicators has been widely used in different regions worldwide. Furthermore, the probabilistic seismic demand model can be used for seismic hazard analysis, reflecting the probability relationship between seismic intensity and demand (Li and Gardoni [2]). As a seismic vulnerability and risk analysis tool, probabilistic seismic demand analysis has been broadly used in seismic engineering research.

Probabilistic seismic risk, empirical observations, and finite element methods are utilized to estimate the seismic vulnerability and damage modal features of RC structures. In addition, numerical simulation analysis can evaluate the performance of structures under various loads or environmental effects, such as earthquake loads, wind loads, and temperature effects, including deformation, stress distribution, vibration characteristics, and corrosion conditions. Simulation analysis helps determine whether a structure's various performance characteristics meet design requirements and is significant for the development and technological progress of structural seismic resistance and seismic risk analysis. Bigdeli et al. [3] conducted a nonlinear time history analysis of typical structures using a finite element model and evaluated selected intensity measures (IMs) through regression analysis. These authors considered criteria such as damage correlation, efficiency, and practicality and generated seismic vulnerability and hazard curves based on modular systems of typical frame structures. They applied them to the establishment of probabilistic seismic demand models. Using nonlinear numerical simulation technology, an improved vulnerability function was proposed by Kim et al. [4], and combined with actual structural damage samples from the 2017 Pohang earthquake in South Korea, a three-dimensional incremental dynamic analysis was conducted. The numerical simulation results were strongly correlated with the damage observation data. Tekeste et al. [5] proposed a method based on Bayesian updating and conducted seismic vulnerability analysis on RC structures through experimental test data (shaking table tests), generating a vulnerability curve model. The fundamental model obtained can improve the accuracy of seismic risk analysis. Boakye et al. [6] developed a critical model for measuring disasters and predicting hazards using a disaster risk assessment framework model. They recommended this approach for assessing the vulnerability and risk of engineering structures. Saed and Balomenos [7] considered the vulnerability of mainshock-aftershock sequences to damage RC structures. They developed a finite element software frame structure model and conducted time history and incremental dynamic analysis. A set of seismic vulnerability comparison curves and surfaces based on different IMs (spectral accelerations) were developed using probabilistic nonlinear algorithms.

Iervolino [8] utilized simplified engineering methods and case studies to develop hazard curves and functions considering probabilistic seismic hazard models. These critical conclusions can contribute to a better understanding and application of probabilistic seismic hazard analysis theory. Iervolino [9] and Iervolino et al. [10] considered the effects of multiple seismic risks, updated and improved the traditional seismic motion prediction equation, and suggested that the proposed model be used to analyze structural seismic risk and vulnerability. Tabandeh et al. [11] developed a model-coupled calculation equation for predicting direct structural earthquake losses by combining seismic risk and resilience quantification methods for industrial buildings. They conducted a case study on the proposed equation using the results of structural numerical model calculations. Blasi et al. [12] used numerical simulation analysis methods and cumulative probability risk models to analyze the collapse vulnerability of RC infill walls and compared RC shear failure in finite element analysis with that in experimental models, and generated vulnerability curves. Sharma et al. [13] calculated the collapse probability of RC structure-filled frames designed based on modern seismic codes in India, taking into account various forms of exposed frames and filled (fully and partially filled) frames, revealing the critical conclusion that the new code's designed frames perform significantly better than the old code. They found that the impact of adding fillers to exposed frames on the probability of collapse is closely related to factors such as design specifications, filler support, relative strength of columns, aspect ratio, and number of floors.

With the rapid development of information technology, machine learning, artificial intelligence, image monitoring technology, fuzzy logic, probability models, and numerical algorithms have been ubiquitously used to estimate the seismic risk and vulnerability of RC structures. Kazemi et al. [14, 15] studied and utilized machine learning algorithms for seismic vulnerability assessment of RC structures and proposed a risk assessment tool that supports reinforcement and design strategies. They also established a prediction model for the seismic response and performance evaluation

of RC frame structures using machine learning methods (Python software). They verified the accuracy of the prediction model using a five-story RC building numerical model. Georgiou et al. [16] selected a typical RC structure in Nicosia, Cyprus, to establish a three-dimensional numerical model. They conducted a comparative analysis of the pushover method and time history based on actual seismic motion characteristics. Zhang et al. [17] developed a model for quickly evaluating the damage status (level) of RC frame structures using machine learning algorithms (random forest, extreme gradient lifting, and active machine learning). They validated the rationality of the developed prediction model using shaking table experimental data. Elyasi [18] innovatively proposed an improved PI evaluation method that utilizes machine learning technology to define damage classification boundaries. Then, they trained and tested the developed classification model using damage survey data from six earthquakes and established a new prediction model for earthquake intensity perception. Bai et al. [19] utilized image monitoring technology to investigate the actual seismic damage of structures and developed an automated structural vulnerability prediction model using deep learning methods. They established a program for image-based damage identification and rapid structural safety assessment of RC components, overcoming the limitations of manual inspection. Li [20] proposed a simplified prediction model for the seismic vulnerability of RC structures using fuzzy sets and decision judgment theory. Fuzzy logic theory was considered by Nale et al. [21], and an innovative proposal was proposed to evaluate the vulnerability of masonry infill walls. The advantages of the proposed innovative model were compared with those of numerical analysis methods.

Research results on the seismic vulnerability of empirical structures significantly impact earthquake risk assessment, building design optimization, and the formulation of seismic fortification standards. Experts and scholars in seismic engineering from different regions worldwide have developed many excellent regional RC structure seismic vulnerability prediction models using various earthquake risk and probability analysis methods based on typical earthquake damage observation data. Using macroseismic IMs as the basis for quantifying the vulnerability of regional RC structures, Del Mese et al. [22] established a regional structural seismic vulnerability model based on the European Macrointensity Scale (EMS-98) and actual seismic damage data from Italian regional structures. Xofi et al. [23] organized the actual seismic damage data of 292,978 RC structures in the Lisbon metropolitan area. They proposed an index-based application to estimate the seismic vulnerability of RC structures. Gioiella et al. [24] proposed an empirical prediction model to estimate the seismic losses of RC buildings based on the research background of RC structure school buildings and historical earthquake damage inspection data in Italy. Jara et al. [25] conducted an analysis of actual seismic damage data from the September 2017 earthquake in Mexico. They used finite element analysis to establish an RC frame structure model and conducted a feature factor analysis on the failure modes of weak story buildings. Sathurshan et al. [26] used a rapid seismic scanning detection method to monitor RC building clusters during the Sri Lankan earthquake. They developed an empirical vulnerability analysis method to predict the seismic vulnerability of RC structures with masonry infill walls. Ko et al. [27] investigated earthquake damage in Taiwan, China, in 2022 and reported the actual seismic damage features of RC structures and revealed the damage mechanism of such structures. Li [28] conducted on-site observations of RC structures that suffered losses during the Wenchuan earthquake on May 12, 2008, in China and proposed a structural vulnerability prediction model based on statistical algorithms (Li and Formisano [29]).

Di Ludovico et al. [30] established a comprehensive, unique database of 2,037 school buildings (damaged and undamaged) by observing the damage situation of RC structures after the 2009 L'Aquila earthquake in Italy. They compared the analysis results of three different methods (empirical methods, empirical–binomial methods, and heuristic methods). They generated vulnerability curves for Italian school buildings (including reinforced concrete (RC) and nonreinforced masonry buildings). Del Gaudio et al. [31] analyzed the damage data of 7,597 RC buildings affected by the 2009 L'Aquila earthquake. By investigating the features of the buildings and the degree of damage to structural and nonstructural components, the damage grade according to the EMS-98 was derived, and a vulnerability curve based on the EMS-98 was derived for the building category. Sagbas et al. [32] performed an actual earthquake damage inspection for a strong earthquake in Türkiye in February 2023, investigated RC buildings in 131 industrial building areas, and developed an empirical seismic vulnerability model of RC structures under the influence of different IMs. Khanmohammadi et al. [33, 34] conducted on-site observations of the Zahab earthquake in Iran and conducted a detailed inspection of the seismic damage of 81 RC buildings, reporting the features and mechanisms of RC structural damage caused by the earthquake event. They proposed an empirical seismic vulnerability model for RC structures based on probabilistic seismic risk and conducted a case study using empirical data from this earthquake event. Li et al. [35–37] conducted a statistical analysis and induced more than 200 actual earthquake damage data points in China. They established an empirical vulnerability matrix model for RC structures based on a database of actual earthquake damage samples. A traditional nonlinear prediction model estimates the probability of seismic failure and the risk of fundamental RC structures.

Formisano et al. [38] conducted an actual seismic damage and risk sequence analysis of building clusters in southern Italy. They developed a new seismic risk model that can be used to estimate the seismic vulnerability of RC buildings. Kassem et al. [39, 40] proposed an improved method for quantifying the seismic vulnerability index and conducted a seismic vulnerability assessment on selected RC structures in Malaysia, establishing a unified criterion. They conducted damage analysis on actual earthquake inspection data and continuously improved the seismic design and specifications. The proposed method can improve the resilience and reliability of buildings and infrastructure and reduce losses and risks caused by earthquakes. Li et al. [41, 42] used China's macroseismic intensity standards [43–45] to process historical earthquake data in China. Combined with on-site observation images, they reported typical seismic damage characteristics of RC structures. They proposed a multifactor quantification method to quickly estimate the actual seismic vulnerability of RC structures. Orntharmarath et al. [46] conducted field inspection and empirical vulnerability analysis on the 2014 Thailand earthquake and established a quantitative model for earthquake risk and vulnerability based on actual damage to regional RC structures. Chieffo et al. [47–49] proposed a multifactor risk quantification method that considers the impact on structural seismic vulnerability and conducted a case study on the model based on actual damage data of building clusters in the Italian region. They considered the impact of vertical seismic motion on structural damage and proposed a damage prediction function that considers the effects of earthquakes in different directions. Zucconi et al. [50] conducted a regional seismic vulnerability analysis of RC buildings and masonry structures in typical regions of Italy, proposed a nonlinear predictive probability model, and generated a vulnerability model based on actual seismic damage datasets. Ruggieri et al. [51–53] and Vukobratović and Ruggieri [54] analyzed the seismic risk and vulnerability of RC building clusters using analytical mechanics-basis estimation methods, and a quantitative model for estimating the seismic vulnerability of regional RC structures was developed. Formisano et al. [55], Chieffo et al. [56] and Mohebi et al. [57] analysed the seismic vulnerability and risk of typical Italian RC buildings using empirical and full-scale testing methods, and a probability model that can be used to predict the vulnerability of regional RC structures was generated.

The above research utilized various methods to study and analyze the seismic risk and vulnerability of RC structures from different perspectives. A large number of functions and models worthy of learning have been developed. However, most related studies are based on analytical model analysis and traditional empirical vulnerability methods, neglecting the correction and optimization effects of numerical simulation methods on vulnerability models of RC structures. In [35] and [37], a vulnerability model was developed based on the probability hazard index by combining actual seismic damage observation data from regional RC structures. However, due to the uncertainty of the capacity and demand parameters of typical structural materials, updating and optimizing the developed structural seismic risk model are argently needed. However, the uncertainty of the capacity and demand parameters of typical structural materials results in insufficient accuracy of the developed seismic risk model, which urgently needs to be updated and optimized. This study innovatively considers the uncertainty of RC structural damage model parameters and combines empirical vulnerability with numerical model analysis methods. We updated the traditional seismic vulnerability model of RC structures using 858 RC structures that suffered varying degrees of damage during the Wenchuan earthquake in China. A typical four-story RC frame structure was selected to establish a finite element model, and vulnerability analysis of multidimensional parameters was conducted. Parameter identification and analysis of the various RC structural damage modes were performed using 117,863 acceleration records obtained from actual seismic station monitoring. Time history curves, engineering demand parameter curves, and damage stress clouds of RC structures in different intensity zones were established to verify the rationality of the developed empirical vulnerability model. The primary focus of the proposed prediction model is on the damage modes and disaster mechanisms of RC structures under different IMs. A nonlinear dynamic time history analysis of acceleration records from multiple stations can effectively and directly reveal different seismic intensity characteristics, contributing positively to obtaining reasonable numerical and empirical vulnerability models. The innovative results obtained are highly consistent with the actual earthquake damage inspection. A set of models can be used to optimize and improve traditional empirical vulnerability models.

2 Seismic failure analysis of RC structures

2.1 Analysis of typical structural failure characteristics

On May 12, 2008, a strong earthquake with a magnitude of 7.9 occurred in Wenchuan County, Sichuan Province, China, causing many buildings to collapse and cause casualties. After the earthquake, the China Earthquake Administration immediately dispatched an expert group to conduct structural damage surveillance on the building structures in the earthquake zone according to the published macroseismic intensity distribution (Fig. 1).

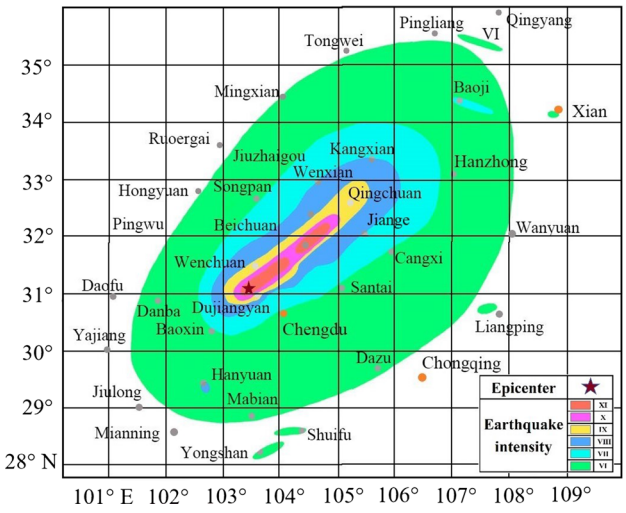

Fig. 1 Seismic intensity distribution of the Wenchuan earthquake in China (May 12, 2008)

Admittedly, RC structures are among the most widely used structural systems worldwide. After actual on-site inspection by the reconnaissance team, it was found that the damage to most RC structures was relatively mild. However, in zones with high intensities or extreme earthquakes, RC structures have experienced severe seismic damage.

According to the actual field observation of earthquake damage, in zones with high intensity or near the macroscopic epicenter, the RC structures experienced group collapses and individual structural failures, as depicted in Fig. 2. Many building samples have experienced varying degrees of damage to infill walls in medium- to low-intensity zones, as reported in Fig. 3. Although infill walls have experienced varying degrees of failure, they have absorbed and consumed some of the seismic energy, indirectly protecting the safety of the main structural system. In addition, some RC structures exhibit shear and axial force coupling effects on the column tops, column bottoms, and beam ends, resulting in varying degrees of failure, as shown in Fig. 4.

To ensure the overall seismic resistance of RC structures, effective connections between different components should be added to improve the overall stiffness of the structure. The role of infill walls should be fully considered to improve their lateral force resistance, strengthen the seismic design of nodes, improve the resistance of columns at the top and bottom, and ensure the seismic performance of columns due to the beam. The role of seismic design and construction should be emphasized, and the quality of the building materials should be improved and ensured.

2.2 Empirical vulnerability optimization model

To explore the actual seismic damage mode of an RC structure and further reveal its damage mechanism and failure characteristics, the China Earthquake Administration sent more than 30 experts to conduct a detailed seismic damage survey in a typical city (Dujiangyan). The field reconnaissance team, including the author, investigated the actual seismic damage of more than 10,000 buildings in Dujiangyan city and collected and established a vulnerability database of actual structures to seismic damage based on the typical city. The RC structure is a typical type of building in a city. The actual seismic damage samples of the RC building cluster investigated were collected, screened, and summarized. We estimated the vulnerability level of all seismic damage samples according to the quantitative scale of the damage level in the latest version of China's seismic intensity standard [45]. A seismic vulnerability dataset based on 858 RC structures was developed. The RC structure samples (858 buildings) used for model verification in this study were obtained from Dujiangyan city. These sample data are randomly distributed in different seismic intensity zones, which makes the developed vulnerability model representative and generalizable. Table 1 shows the disaster matrix considering the number of earthquake damage investigations and the corresponding ratio. It is worth noting that the five levels of damage are roughly intact (DS1), slightly damaged (DS2), generally damaged (DS3), significantly damaged (DS4), and partially or overall collapsed (DS5). The damage ratio is the number of samples with different vulnerability levels in each intensity zone divided by the total number of samples. Figure 5 demonstrates the vulnerability and damage distribution of the RC structure in Dujiangyan city. The actual structural probability damage function (Eq. 1) can estimate the degree of damage to the structure at different failure levels, and this function can quickly and accurately estimate the structural damage characteristics in zones of different intensities.

$$P[DP_i|IM] = P[DS_i \le ds_i|IM] \tag{1}$$

IM represents seismic intensity measures (macroseismic intensity). $P[DP_i|IM]$ is the probability of the i-th level damage of the RC structure under a given IM action. $P[DS_i \le ds_i|IM]$ is the cumulative failure probability of the RC structure reaching or exceeding the i-th failure level DS_i under a given IM.

Nonlinear vulnerability regression analysis is crucial for predicting the seismic risk and vulnerability of typical building structures. Chieffo et al. [47] [48] and Formisano et al. [38] processed and analysed actual seismic damage data from typical European building structures

(a) Overall failure of the building cluster

(b) Overall collapse

(c) Overall failure of a single structure

(d) Partial failure of single structure

(e) Complete failure of the bottom layer of the structure

Fig. 2 Overall or local failure of RC structure

and proposed a logarithmic normal distribution function (LNDF) model that can predict the seismic vulnerability of typical structures, as expressed in Eq. 2. They used typical structural seismic damage data from Italy to verify the rationality of the vulnerability prediction model. Del Gaudio et al. [31] conducted an actual vulnerability

(a) Partial failure of infill wall

(b) Cracking and local collapse of infill walls

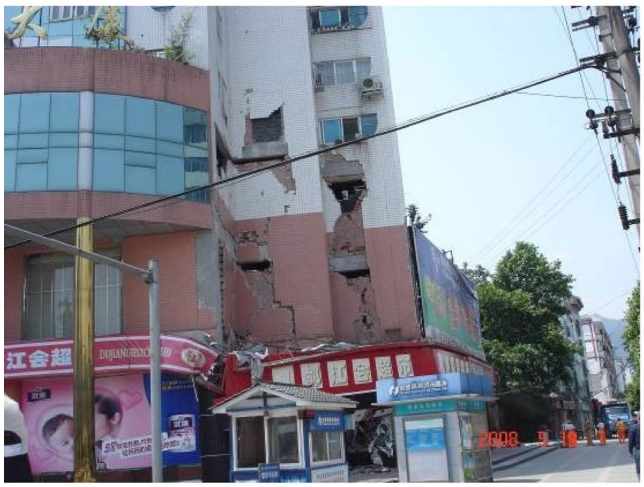

(c) Severe cracking of the infill wall

(d) Partial failure of longitudinal and transverse infill walls

Fig. 3 Failure of infill walls in RC structures

analysis of RC buildings affected by the 2009 L'Aquila earthquake in Italy. They proposed an exponential-based nonlinear prediction function (EBNPF) to estimate the seismic risk and vulnerability characteristics of RC structures, as expressed in Eq. 3. Li et al. [35, 41, 58–61] developed a nonlinear fitting model using the old version of China's seismic intensity scale. They used earthquake damage data from China to predict and estimate the model. However, the intensity measurements of the developed RC vulnerability prediction models are outdated, and the estimation accuracy is uncertain, indicating that an established seismic risk model urgently needs improvement. Based on existing seismic risk probability models and nonlinear regression algorithms, this paper develops a Gaussian nonlinear regression function (GNRF) using the latest Chinese seismic intensity standard to estimate the actual seismic risk and vulnerability of RC structures, as expressed in Eq. 4. Using the established updated RC structural vulnerability database and matrix, structural vulnerability prediction curves based on the damage ratio (DR) for different intensity zones were developed, and the vulnerability quantification parameter matrix based

(a) Failure of the top of the frame column

(b) Failure of the bottom of the frame column

(c) Shear failure of the frame beam

Fig. 4 Failure of typical structural components

Table 1 Disaster matrix considering actual structural seismic damage observation data (RC buildings)

Seismic intensity zone	Number of inspections and damage ratio (survey quantity and damage ratio (DR))					
	DS1	DS2	DS3	DS4	DS5	Total
VI	210/0.89	22/0.09	3/0.02	0/0	0/0	235/1
VII	134/0.68	45/0.22	17/0.09	1/0.01	0/0	197/1
VIII	63/0.25	101/0.4	62/0.25	26/0.1	0/0	252/1
IX	17/0.1	28/0.16	37/0.22	72/0.41	20/0.11	174/1
Overall	424/0.49	196/0.23	119/0.14	99/0.12	20/0.02	858/1

on actual seismic damage data was calculated, as shown in Fig. 6 and Table 2.

$$P(DS_i \geq ds_i|IM) = \Lambda\left[\frac{\ln(IM) - \omega}{\xi}\right] = \Lambda\left[IM,\ \alpha_1,\ \alpha_2 \cdots \alpha_n\right] \tag{2}$$

$\Lambda[\bullet]$ is a traditional logarithmic normal distribution function model. ω and ξ are the mean and variance, respectively, based on the function model. $P(DS_i \geq ds_i|IM)$ is the conditional probability based on traditional macroseismic intensity measures that the RC structure cluster reaches or exceeds the specified damage states ds_i. i is an integer from 1 to 5, representing five expanded vulnerability levels.

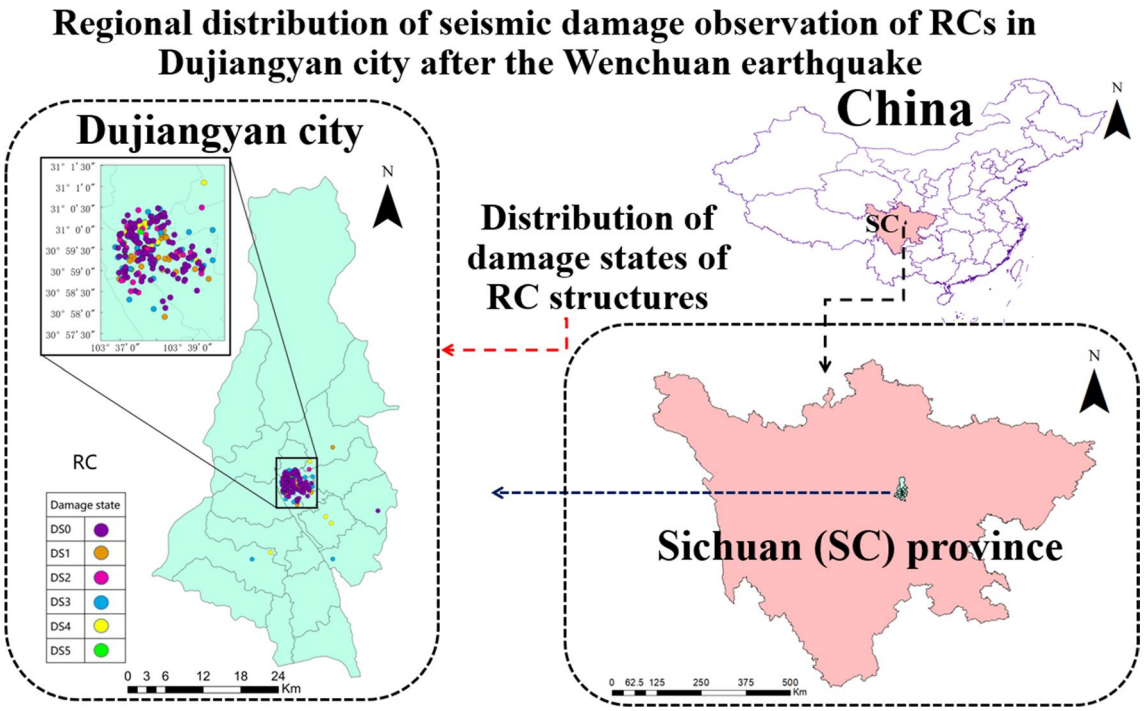

Fig. 5 Seismic damage observation and vulnerability distribution of RC structures in Dujiangyan City

$\alpha_1, \alpha_2 \cdots \alpha_n$ are n regression feature coefficients based on empirical RC structure actual earthquake damage sample data.

$$P(DS_i \geq ds_i|IM) = \Psi\,[IM,\ \beta_1,\ \beta_2,\ \cdots \beta_n] = 1 - e^{-\psi \bullet IM^{\zeta}} \tag{3}$$

$\Psi[\bullet]$ is an exponential basis continuous distribution function. ψ and ζ represent the damage estimation parameters for the RC structures. $\beta_1, \beta_2, \cdots \beta_n$ are n regression feature coefficients that consider the exponential-based continuous distribution function of the actual RC structure earthquake damage database.

$$P(DS_i \geq ds_i|IM) = \Phi\,[IM,\ \gamma_1,\ \gamma_2,\ \cdots \gamma_n] \tag{4}$$

IM represents a discrete seismic intensity measure (macroseismic intensity) used to predict the seismic vulnerability and risk of RC structures. $\Phi[\bullet]$ is a Gaussian nonlinear regression function model that considers the vulnerability level of RC structures. $\gamma_1, \gamma_2, \cdots \gamma_n$ represent n objective regression coefficients based on the empirical failure dataset of RC structures.

According to the vulnerability assessment models of RC structures in different seismic intensity zones, in zone VI, the similarity of the EBNPF and GNRF curve changes is relatively high, and the goodness of fit is relatively high (both reaching 1), which is slightly greater than the prediction curve accuracy of the LNDF. The damage to RC structures is relatively mild. In zone VII, the maximum value of the curve at the DS1 level indicates a decreasing trend, while the DR value at the DS3 level significantly increases. The RC damage is inconspicuous, and the actual field inspection results mostly reveal slight damage to the nonstressed components. In zone VIII, the damage to the RC structure worsens, and the goodness of fit of the GNRF is slightly greater than that of the EBNPF and LNDF. Some RC structures have relatively high DR values at the DS2 and DS3 levels, and the proportion of DS4 begins to increase. In zone IX, the prediction accuracy (goodness of fit) of the EBNPF and GNRF is significantly greater than that of the LNDF, and there is a significant increase in RC structures at the DS4 and DS5 levels. It is worth emphasizing that there are still some samples with DS1 and DS2 damage levels, and actual field observations indicate that RC structures designed for seismic resistance can still maintain good seismic resistance in high-intensity zones. After extensive regression analysis and testing of actual seismic damage data from RC structures, the results indicate that the Gaussian distribution has a relatively sensible goodness of fit and regression ability. Overall, the damage to the RC structure in the seismic zone is relatively mild, and the prediction accuracy and goodness of fit of the three prediction models are similar. The RC structure samples used for model verification in this paper were taken from the overall field survey database of Dujiangyan city, which contributed to the rationality of the developed model.

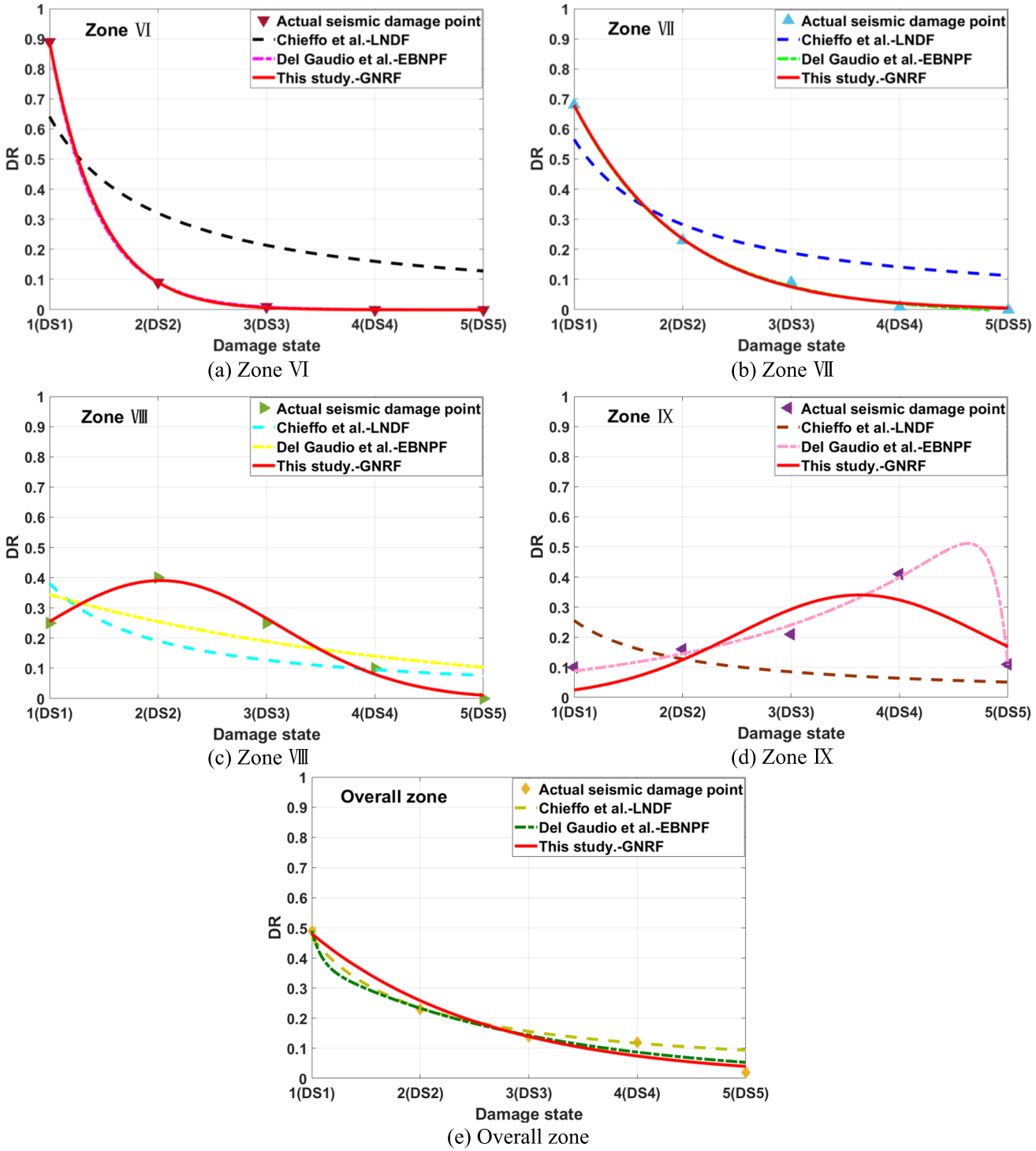

Fig. 6 Seismic fragility curve of RC structures considering cumulative exceedance probability (CEP)

3 Numerical model of the RC structure

With the development of computer technology and numerical simulation methods, the finite element method has become essential for studying the seismic damage and vulnerability of RC structures. Large-scale general finite element software has significant advantages in the nonlinear analysis of structures and has led to its widespread application in simulating the seismic damage and vulnerability of structures. According to field observations of the actual

Table 2 Fragility and hazard undetermined parameter matrix considering the empirical RC structure damage dataset

Intensity zone	Nonlinear regression model														
	Chieffo et al. [47] [48]				Del Gaudio et al. [31]						This Study				
	LNDF/α_n			Goodness of fit	EBNPF/β_n				Goodness of fit		GNRF/γ_n			Goodness of fit	
	α_1	α_2	α_3		β_1	β_2	β_3	β_4			γ_1	γ_2	γ_3		
VI	0.664	0.4037	0.9544	0.6711	-1.546×10^{-5}	0.5529	8.789	− 2.29	1		1.091×10^{4}	− 7.716	2.841	1	
VII	0.6712	0.693	0.9751	0.8258	− 0.001839	0.3956	1.945	− 1.048	0.9991		799	− 12.81	5.192	0.9986	
VIII	0.5482	0.4752	0.5256	0.1367	0.4635	− 0.2992	0	0	0.516		0.3903	2.025	1.57	0.9909	
IX	0.3206	1.423	2.223	-1.568	0.05292	0.5054	-1.013×10^{-16}	7.247	0.9774		0.3404	3.634	1.632	0.615	
Overall	0.5146	0.1656	0.7946	0.9515	6247	− 10.95	0.6224	− 0.4912	0.9827		3.547×10^{66}	− 496.5	40.09	0.9736	

RC structures of the Wenchuan earthquake in China, these structures exhibit various seismic damage features under the influence of different intensities of seismic motion. To further investigate the damage modes and failure mechanisms of RC structures, this study selected a typical four-story RC frame structure in an actual earthquake zone and constructed the model at a 1:1 ratio. We thoroughly considered the tensile stiffness effect of concrete, the confinement effect of hoops, and the constitutive relationship between concrete and steel bars. We conducted numerical simulations on the damage features of the four-story RC frame structure under different seismic IMs. The feasibility of the research method was verified based on actual structural seismic damage observations.

3.1 Unit types and material dynamic constituents

The floor slab of the RC frame structure is constructed and simulated using "Solid" units provided in software, with a type of C3D8R, and a single steel bar is constructed using linear wire units, with a type of B31. The steel reinforcement skeleton adopts truss frame elements, and the type of fibre beam element is T3D2. The steel reinforcement is established using the truss method. That is, the steel reinforcement skeleton is first constructed, and then the material properties are assigned. Both the frame beams and columns are modeled using "Solid" units, and the steel skeleton is embedded into the concrete using a "Tie" connection method without a common node method. The constructed unit is based on the Timoshenko beam theory, considering the influence of shear deformation stiffness. The beams, slabs, and columns are all made of C30 concrete. The stirrups of the beams and columns use an HPB300, and the longitudinal bars use an HRB335. The board adopts HPB300 and HRB335.

The uniaxial stress–strain relationship evaluation curve of concrete models can reflect the constraint effect and softening behavior under loading. In contrast, the unloading and loading curves can reflect the hysteresis and stiffness degradation characteristics of materials under repeated loading. By combining the constitutive relationships of concrete and steel bars in the Chinese Code for Design of Concrete Structures (GB50010-2002), stress–strain curve models are calculated and generated through the constitutive equations of concrete under uniaxial compression and tension (Eqs. 5–8), as shown in Fig. 7, where ε_u is the compressive strain of concrete when the stress on the descending section of the stress–strain curve is equal to $0.5f_c^*$.

$$x \le 1, y = \alpha_a x + (3 - 2\alpha_a)x^2 + (\alpha_a - 2)x^3 \quad (5)$$

$$x > 1,\ y = \frac{x}{\alpha_d(x-1)^2 + x},\ x = \frac{\varepsilon}{\varepsilon c},\ y = \frac{\sigma}{f_c^*} \tag{6}$$

α_a and α_d are the parameter values for the rising and falling segments of the uniaxial compressive stress–strain curve, as shown in Table 3. f_c^* is the uniaxial compressive strength of the concrete (f_{ck}, f_c, or f_{cm}). ε_c represents the compressive strain value of the concrete corresponding to f_c^*. x is the ratio of strain to peak strain, with a range of values less than 0.5 f_t^* and greater than 0. σ and ε are the stress and strain values of the concrete, respectively.

$$x \le 1,\ y = 1.2x - 0.2x^6 \tag{7}$$

$$x > 1,\ y = \frac{x}{\alpha_t(x-1)^{1.7} + x},\ x = \frac{\varepsilon}{\varepsilon_t},\ y = \frac{\sigma}{f_t^*} \tag{8}$$

α_t represents the parameter value of the descending section of the uniaxial tensile stress–strain curve. f_t^* is the uniaxial tensile strength of the concrete (f_{tk}, f_t, or f_{tm}). ε_t is the tensile strain of the concrete that matches f_t^*.

According to the values and limitations of the material characteristic parameters in software, the strain values under compression and tension are limited to a range of $0.6\varepsilon_{c/t}$ to $3\varepsilon_{c/t}$. The value of the concrete damage parameter $d_{c/t}$ should be above 0.95. The true stress and strain values of the concrete were calculated, and a relationship curve was generated, as shown in Fig. 8.

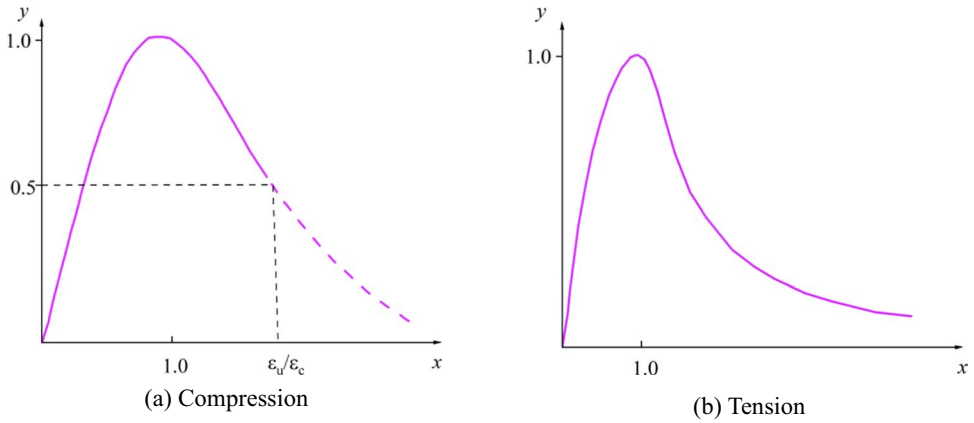

Fig. 7 Stress–strain curves under uniaxial compression and tension

Table 3 The parameter values of the constitutive relationship of concrete (C30)

f_c^* (N/mm^2)	E (MPa)	ε_c (10^{-6})	α_a	α_d	f_t^* (N/mm^2)	ε_t (10^{-6})	α_t
30	3×10^4	1640	2.03	1.36	2.0	95	1.25

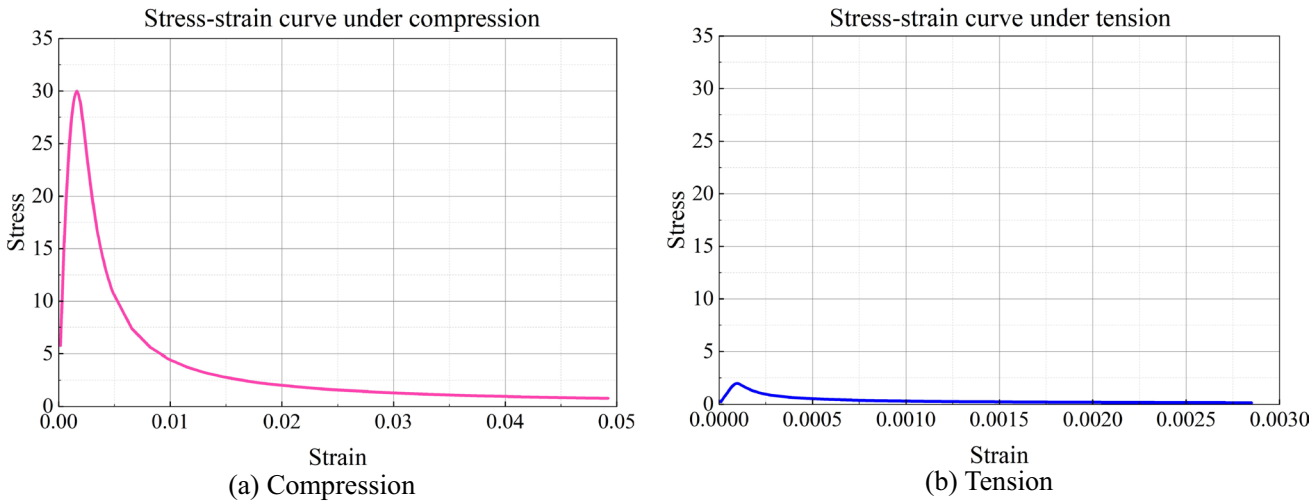

Fig. 8 Stress–strain relationship curve of concrete under real compression and tension

According to the Chinese Code for Design of Concrete Structures [62] and the selection of material characteristic parameter values, considering the irreparable deformation of materials (damage factors inherent in the material itself), the calculation of concrete damage factors and the determination of nonelastic strain values can be calculated according to Eq. 9, thereby obtaining the true stress–strain relationship of concrete. It is worth emphasizing that it is impossible to recover according to the initial elastic modulus when the material undergoes deformation, and the material should be recovered according to $(1\text{-}d)\times E_0$. Therefore, the input values in software are the true stress and nonelastic strain values. In addition, according to the concrete damage plasticity model (Fig. 9) [62], during the tensile stage of concrete (from O to A), the initial elastic modulus E_0 reaches the tensile strength (σ_{to}) of the concrete, causing failure and the stress to decrease to B. After stopping loading, the concrete recovers according to the elastic modulus of $(1\text{-}d_t)\times E_0$ and reaches point C. Under the cyclic load of tension and compression, the concrete is compressed from C to D again and stops loading after reaching an estimated strength. At this point, the elastic modulus $(1\text{-}d_t)\times(1\text{-}d_c)\times E_0$ can be restored to further obtain the constitutive characteristic relationship of the concrete.

$$d = 1 - \sqrt{\frac{\sigma}{E_0\varepsilon}},\ \varepsilon^{in} = \varepsilon - \varepsilon^{ol},\ \varepsilon^{ol} = \frac{\sigma}{E_0},\ \varepsilon^{pl} = \varepsilon^{in} - \frac{d}{1-d}\cdot\frac{\sigma}{E_0} \tag{9}$$

d represents the damage factor. σ and ε are the actual stress and strain of the concrete, respectively. ε^{in} represents the nonelastic strain value of the concrete. ε^{ol} is the strain value recovered according to the initial elastic modulus. ε^{pl} is an irreversible nonelastic strain that increases and is not zero.

The constitutive relationship of the steel bars is estimated using a double-line model, which fully considers the isotropy and strain rate effects of the steel. It is widely used in the elastic–plastic seismic response analysis of RC and steel structures. Using Eq. 10 and the line theory method, the stress and strain relationship of the steel bars was calculated, and a double-line model of the steel bars was generated, as shown in Fig. 10.

$$E_s'' = 0.01E_s,\ \varepsilon_y = \frac{\sigma_y}{E_s},\ \varepsilon_u = \varepsilon_y + \frac{\sigma_u - \sigma_y}{E_s} \tag{10}$$

E_s is the initial elastic modulus. E_s'' represents the elastic modulus after yielding. σ_y and ε_y represent the yield stress and strain, respectively. σ_u and ε_u are the ultimate stress and strain, respectively.

Note that the strain provided by the plastic properties of steel bars includes the material's plastic strain and the material's overall strain. Therefore, the overall strain should be decomposed into elastic and plastic components for consideration. The elastic strain equals the ratio of the true stress to Young's modulus. The plastic strain is the total minus the elastic strain, as expressed in Eq. 11.

$$\varepsilon^{pl} = \varepsilon^{t} - \varepsilon^{el} = \varepsilon^{t} - \frac{\sigma}{E} \tag{11}$$

ε^{pl} represents the true plastic strain. ε^{t} is the true strain of the whole. ε^{el} is the true elastic strain.

Based on the stress and plastic strain of the steel bars in the yield and limit states, the above calculation model was used to calculate the RC frame structure, and the constitutive

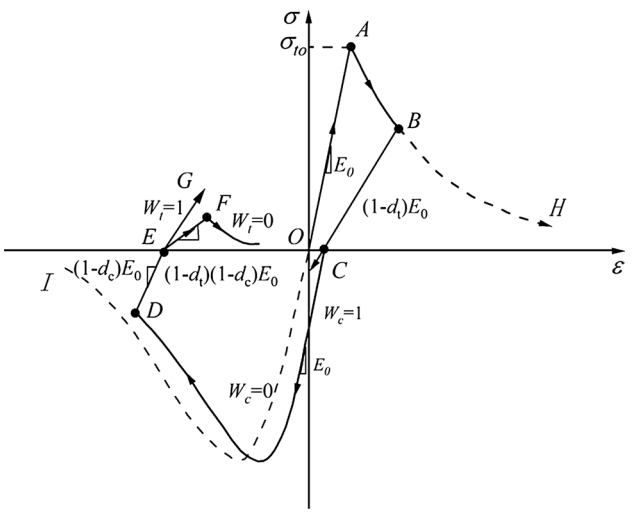

Fig. 9 Damage plasticity model of concrete

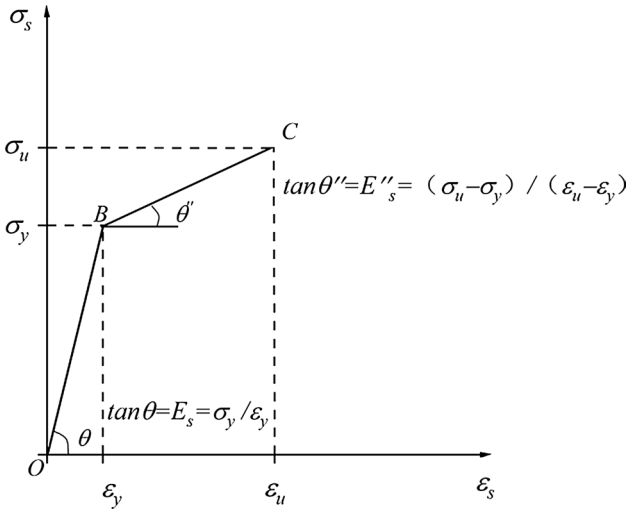

Fig. 10 Bilinear model of steel reinforcement

relationships of the steel bar categories used were obtained, as shown in Table 4.

3.2 Construction of structural models

A typical four-story RC frame structure in Dujiangyan city is selected as the research object, and a three-dimensional finite element model is established. The structure has a height of 14.4 m, with a floor height of 3.6 m, a total plane length of 48.9 m, and a width of 16.8 m. According to the Chinese Code for Design of Concrete Structures, the site category is selected as Class 2. The safety level of the building is Grade 2, with a design service life of 50 years. The seismic fortification category is Class B, the seismic fortification level of the frame is Grade 4, the seismic fortification intensity is Degree 7, and the design basic seismic acceleration is 0.05 g. The maximum dimensions of the frame beams, slabs, and columns are $600 \times 800 \times 9000$ mm, $6000 \times 6900 \times 150$ mm, and 400×1000 mm, respectively. The PGA amplitudes in zones VI to IX are 18 cm/s, 35 cm/s^2, 70 cm/s^2, and 140 cm/s^2. The size of the developed model is a 1:1 full-scale model, and the plane, facade, and maximum cross-sectional reinforcement of the RC structure are depicted in Fig. 11. Figure 12 shows the three-dimensional spatial model of the four-story RC frame structure.

The feature parameters of seismic motion (acceleration) are the core quantitative indicators for estimating the seismic response and vulnerability of structures. To obtain relatively accurate seismic risk and vulnerability features of RC structures, 901,530 real acceleration records monitored by eight seismic stations were selected. By combining the dynamic time history and algorithm, nonlinear dynamic time history and response spectrum curves based on real seismic station monitoring data were generated (EW, NS, and UD represent the east–west, north–south, and up and down directions, respectively. ζ is the damping ratio), as shown in Figs. 13 and 14.

Table 4 Calculation results of the constitutive relationships for the different types of steel bars

Rebar type	State	Strain	Stress	Elastic modulus	Plastic strain
HPB300	Initial	0	0	2.10E+05	0
	Yield	1.43E-03	300	2.10E+05	0
	Ultimate	5.86E-02	420	2.10E+05	5.71E-02
HRB335	Initial	0	0	2.00E+05	0
	Yield	1.68E-03	335	2.00E+05	0
	Ultimate	6.17E-02	455	2.00E+05	6.00E-02
HRB400	Initial	0	0	2.00E+05	0
	Yield	2.00E-03	400	2.00E+05	0
	Ultimate	7.20E-02	540	2.00E+05	7.00E-02

4 Numerical simulation analysis

4.1 Analysis of seismic demand parameters

To study the dynamic features and damage modes of RC structures under the influence of floor factors and different IMs, this study used numerical simulation analysis methods to conduct nonlinear dynamic analysis considering the impact of floor factors, taking the story drift as the demand parameter. Combining the dynamic time history and structural response calculation results, a comparison curve was obtained for the dynamic response of RC structure floors in different intensity zones, as shown in Fig. 15.

According to the identification and analysis of the dynamic parameters of the model, the calculated interlayer displacement angle of the Y-axis is smaller than that of the X-axis. We combine the limit value of the story drift (1/550) of RC frame structures in the Chinese Concrete Structure Design Code [62] to determine the damage level of the structure. In zone VI, the maximum story drift reached 0.000045, which can be determined to be basically intact (DS1). In zones VII and VIII, the calculation results of story drift reveal that there is little difference between the two zones, with the maximum story drifts reaching 0.000197 and 0.00016, respectively. The damage level can be determined as minor damage (DS2). In zone IX, the maximum story drift reaches 0.000509, indicating a moderate damage level (DS3), which is consistent with the seismic damage state obtained using empirical vulnerability and macroscopic intensity quantification methods.

Incremental dynamic analysis (IDA) is a parameterized analysis method used to evaluate the performance of structures under seismic action. The IDA method performs a certain proportion of amplitude modulation on ground motion records and uses the processed ground motion parameters as structural inputs for dynamic time history calculations. The seismic damage of the structure is estimated by analyzing the engineering requirement parameters. This study combines IDA and the uncertainty of seismic input to collect seismic parameters obtained from actual monitoring stations during the Wenchuan earthquake in China. Based on the PGA value specified in the Chinese seismic intensity standard as the strength index and with the story drift and interlayer stiffness as performance parameters, damage mode estimation and analysis were conducted on the developed RC structural model. Based on the author's field inspection of the seismic damage situation of RC structures, we selected typical points (column top, mid-span of the beam, one-third of the beam, and quarter of the beam, as shown in Fig. 16) on floors 1–4 subjected to composite stress for engineering requirement parameter analysis and established a dynamic

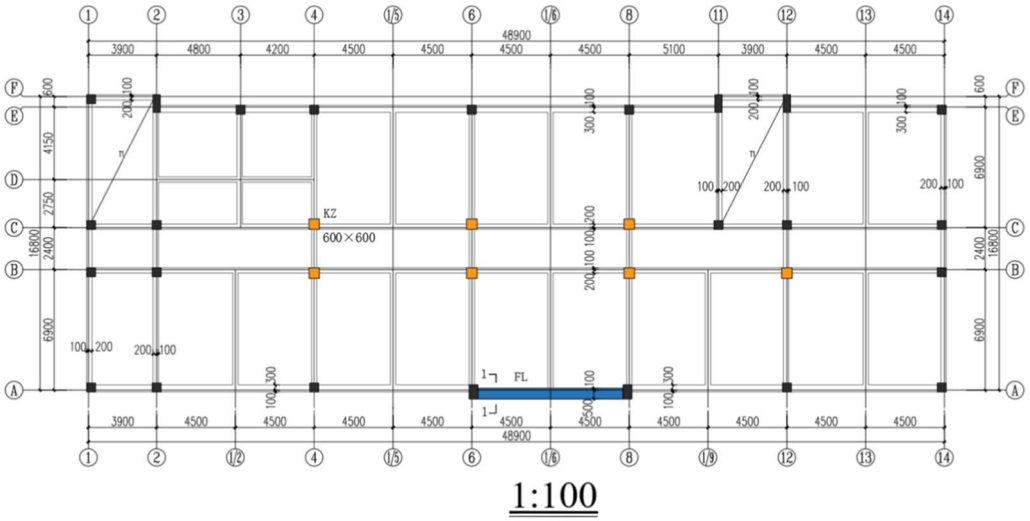

(a) Plane layout

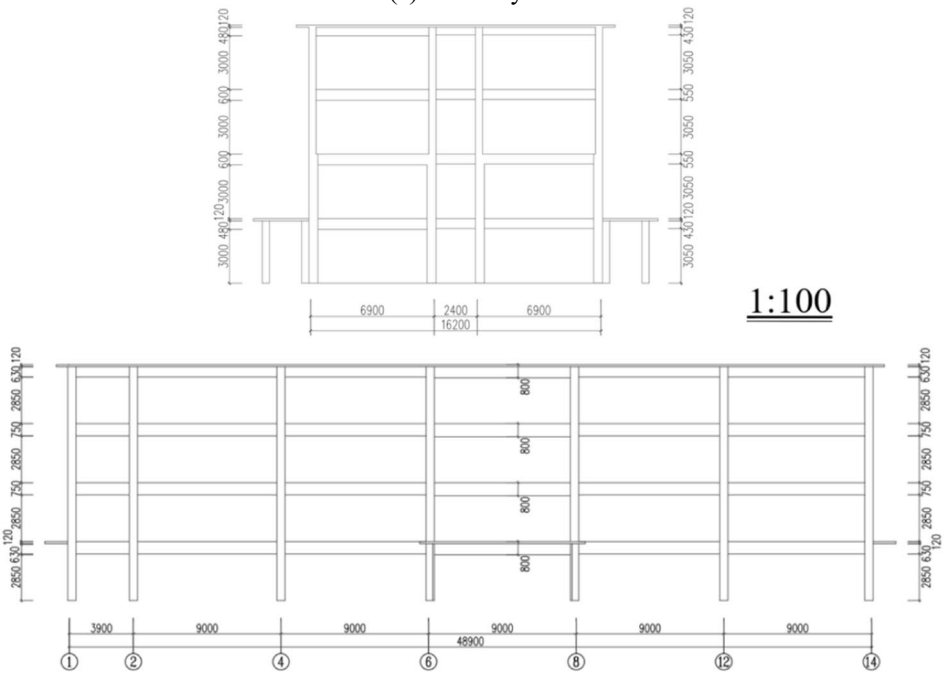

(b) Facade layout

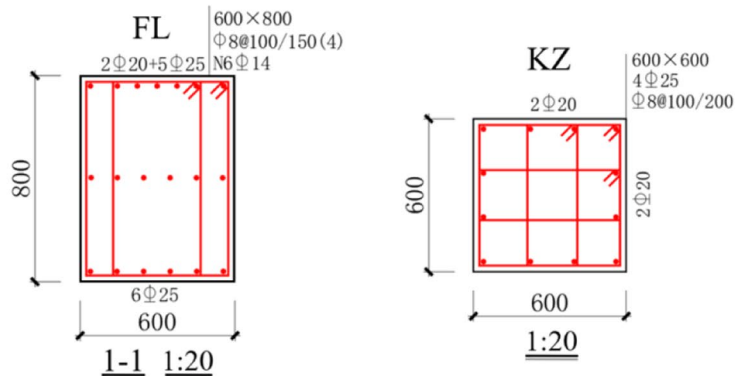

(c) Typical beam and column cross-section layout

Fig. 11 The structural layout of the RC frame (mm)

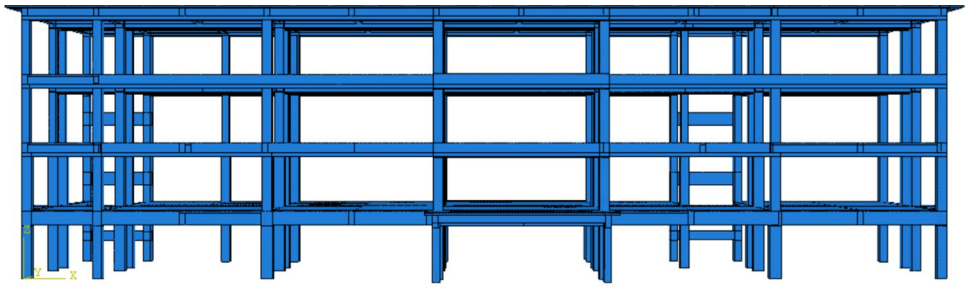

(a) Facade

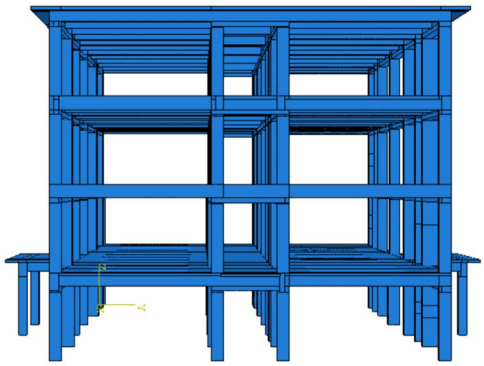

(b) Side elevation

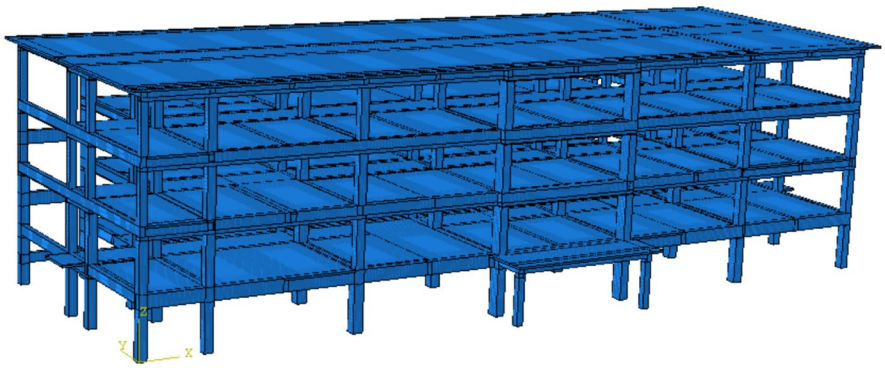

(c) Panorama

Fig. 12. 3D model layout of the RC frame

damage curve based on the story drift and interlayer stiffness, as depicted in Figs. 17, 18, 19, 20.

According to the calculation results of the interlayer stiffness of the structure, in zone VI, the interlayer stiffness at KL8 on the fourth floor of the RC frame structure is the highest, with a value of 9.626 kN/m. The interlayer stiffness values at KL8 on the bottom and third layers are 7.3 kN/m and 8.833 kN/m, respectively. The interlayer stiffness at KL8 on the second floor is 6 kN/m, which is lower than that at KL8 on the bottom and third floors. The interlayer stiffness of RC frame structures KL8 and KL9 is relatively high, while the interlayer stiffness of KL1, KL5, and KL10 is relatively small. According to the calculation results of the story drift of the frame beam, it can be concluded that the story drifts at KL1, KL5, KL8, KL9, and KL10 on each floor of the RC frame structure are relatively large under the influence of intensity measure IX. The maximum story drift at KL8 on the second floor of the RC frame structure is 6.857×10^{-4} rad. The story drifts at KL8 on the bottom and third floors are 5.48×10^{-4} rad and 5.28×10^{-4} rad, respectively, which are small differences. The story drifts at KL8 on the fourth floor are the smallest, with a value of 2.856 rad.

According to the analysis results of the interlayer stiffness, under the influence of intensity measure VI, the interlayer stiffness at KZ2-2 on the fourth floor of the RC frame structure is the highest, with a value of 10.052 kN/m. The interlayer stiffness values at KZ2-2 in the second and

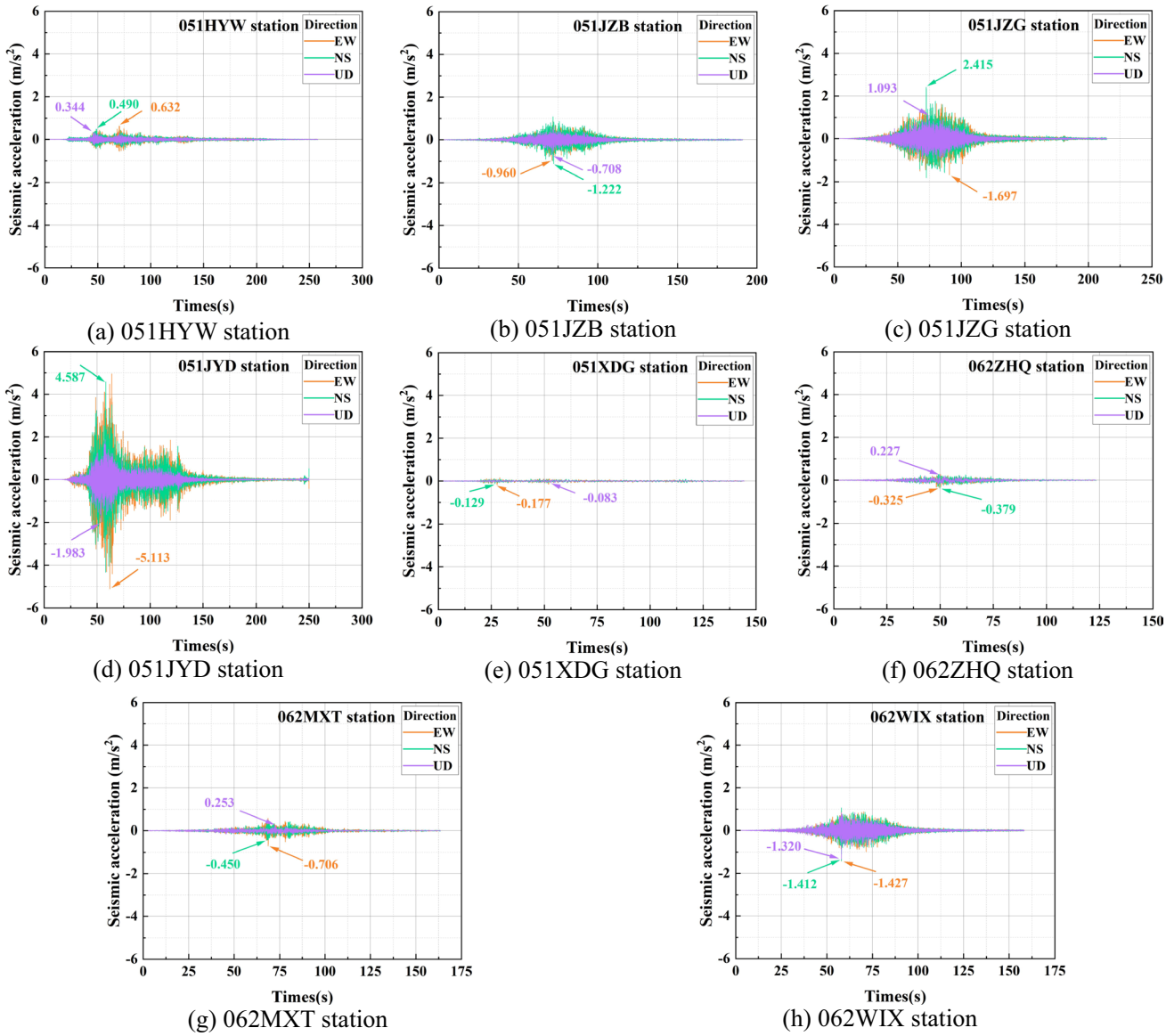

Fig. 13 Nonlinear dynamic time history curves (Wenchuan earthquake in China)

third layers are 4.955 kN/m and 4.354 kN/m, respectively, which are slightly different. The interlayer stiffness at the bottom layer KZ2-2 is 5.774 kN/m, which is greater than that at the second and third layers KZ2-2. The interlayer stiffness of KZ2-1 and KZ2-2 on the first to third floors of the RC frame structure is relatively high. In contrast, the interlayer stiffness of KZ1-1, KZ3, and KZ1-2 is relatively low, indicating that the interlayer stiffness at the middle position of the structure is relatively high. The interlayer stiffness at the edge position is relatively low. According to the calculation results of story drift, in zone IX, the story drifts at KZ1-1, KZ2-1, KZ2-2, KZ3, and KZ1-2 on each floor of the RC frame structure are relatively large. The story drifts at KZ1-2 on the second floor of the structure are the greatest, with a value of 5.225×10^{-4} rad. The story drifts at KZ1-2 on the bottom and third floors are 4.180×10^{-4} rad and 4.140×10^{-4} rad, respectively. The story drifts at KZ1-2 on the fourth floor are the smallest, with a value of 2.325 rad. According to the Chinese seismic design code requirements for buildings, the limit value of story drift for RC frame structures is 1/550. The results obtained from the numerical simulation calculations all comply with the needs of the seismic design code. In this paper, seismic motion parameters of different intensities were selected according to the Chinese seismic intensity standards, and model input and dynamic response analysis were conducted. The results indicate that the model has good robustness under different sequences. It is worth emphasizing that the sensitivity of

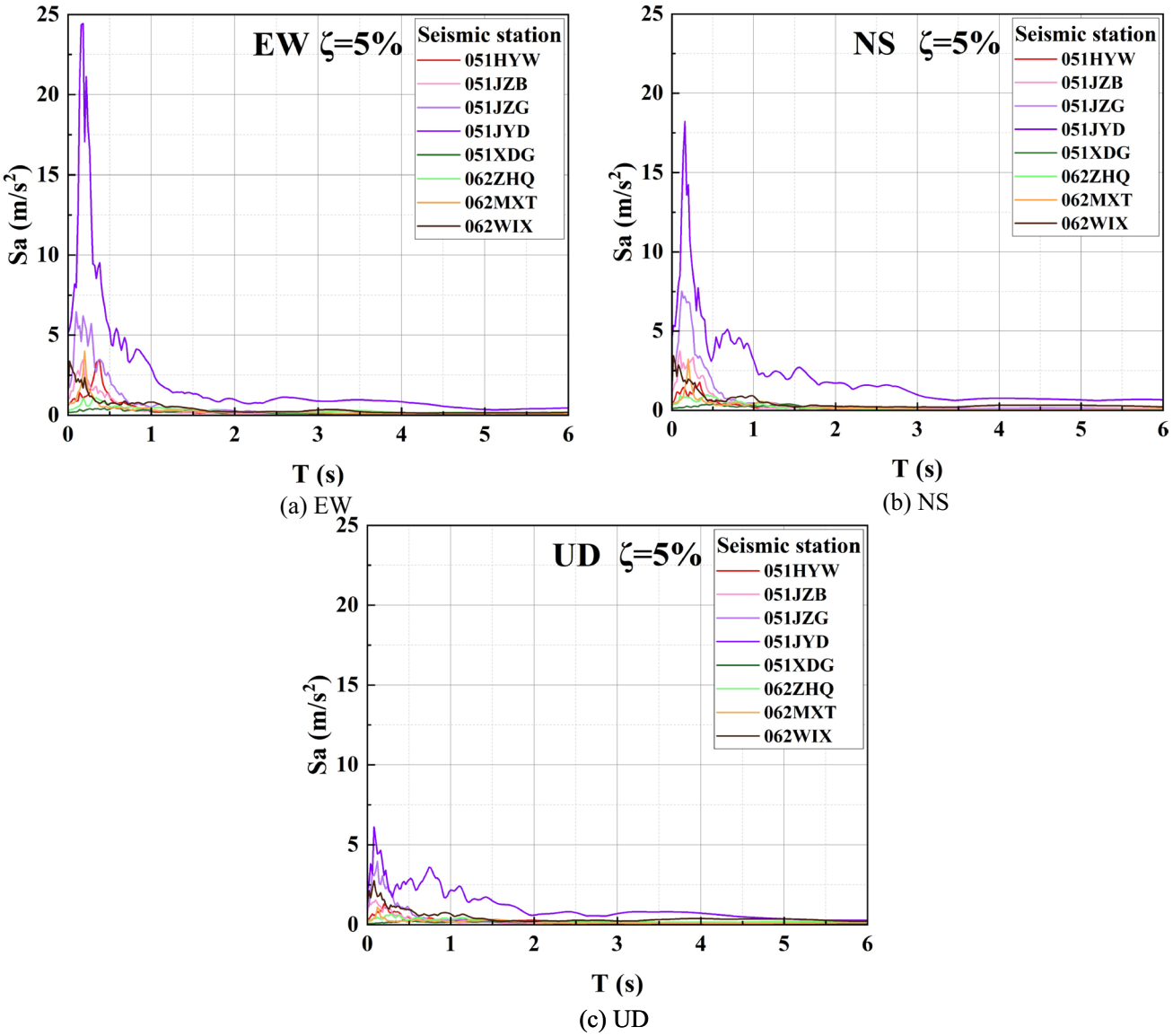

Fig. 14 Seismic response spectrum based on real acceleration monitored by eight seismic stations

the model to the input variable (seismic acceleration) is relatively weak, ranging from 0.45 to 1.77 m/s^2, while it is relatively significant, ranging from 1.78 to 7.07 m/s^2.

4.2 Dynamic time history analysis

According to actual seismic damage observations of RC structures, different IMs and excitations have significant differences in their seismic responses. Moreover, the damage caused by ground motion to different floors of RC structures also has other characteristics. To study the seismic response of RC structure floors to ground motions of different intensities, we processed 117,863 acceleration records monitored by the China Earthquake Networks Center. We conducted amplitude modulation according to the acceleration value range of zones VI–IX in the latest version of the China Seismic Intensity Standard. The processed seismic parameters were applied separately to the developed RC frame structure model, and a large number of numerical calculations were conducted. The damping coefficient of the structure is calculated based on the structure's natural frequency, considering mass damping and stiffness damping. The material damping is set according to C30 concrete damping, while the damping coefficient of the steel reinforcement is set according to different strength levels. Based on the calculation data obtained from the model analysis, the dynamic time history curves of layers (1–4) under the influence of different seismic IMs were established (framed columns), as shown in Figs. 21, 22, 23, 24.

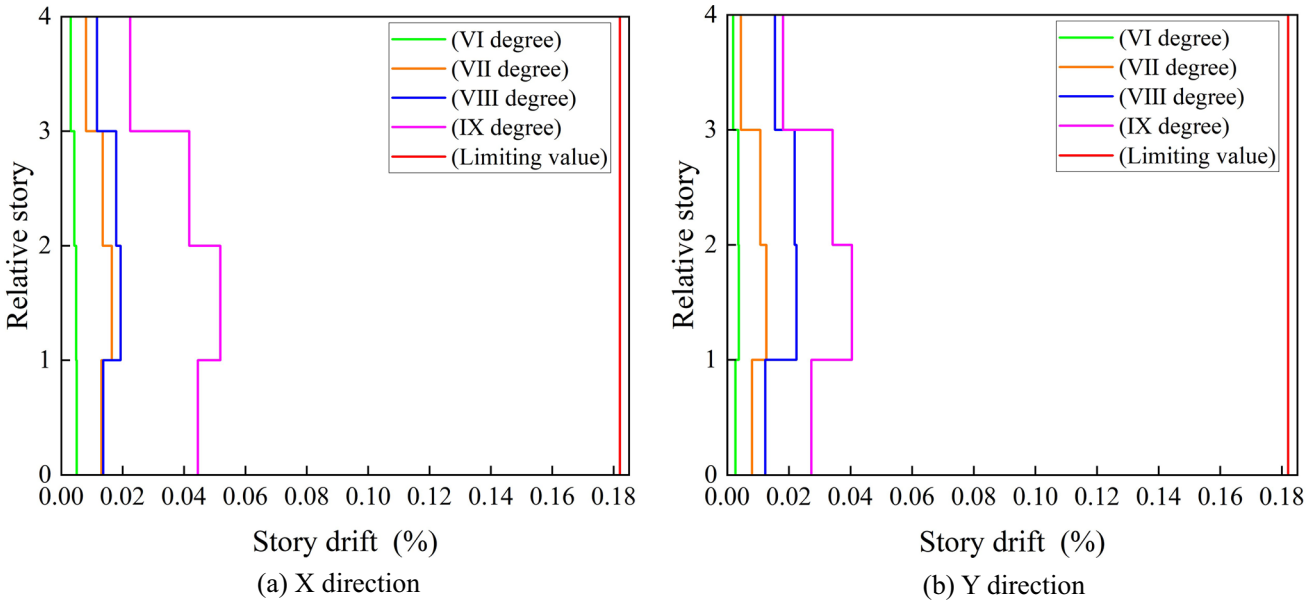

Fig. 15 Story drift of RC structure considering the influence of different intensity measures

The dynamic time history analysis of the RC structural model used 1177.4 s (288.5 s in zone VI, 246.4 s in zone VII, 326.5 s in zone VIII, and 316 s in zone IX), and the dynamic features from the 1st to 4th floors under the influence of different IMs were compared. According to the numerical simulation and time history analysis results of the RC structural model, in zone VI, the difference in the seismic response characteristic parameters of each layer is relatively low, indicating that the impact of lower IMs on different floors of the structure is relatively small. In zone VII, the peak seismic acceleration of the fourth layer is significantly greater than that of the first and second floors, and the dynamic response of the upper floors is relatively significant. In zone VIII, the difference in the seismic response feature parameters of each layer is not significant, and the peak seismic acceleration of each layer is lower than that in zone VII, indicating that the RC structures have a certain degree of flexibility and resilience. In zone IX, the peak amplitude of the acceleration on each floor significantly increases. The difference in the seismic response characteristic parameters of each layer is also relatively low, and the peak seismic acceleration of the second layer is smaller than that of the other layers.

4.3 Structural damage cloud analysis

To investigate the damage modes and differential characteristics of multiple floors of RC frame structures under the influence of different seismic IMs, we processed 117,863 real earthquake accelerations obtained from Wenchuan earthquake monitoring. We limited the acceleration values to different intensity zones according to the Chinese seismic intensity standards. The damage to the concrete and steel bars under different seismic IMs was considered separately, and the structural component parameters were determined for the concrete and steel bars. Using numerical simulation and the Moire algorithm to simulate the damage of RC structural models affected by different seismic IMs. A set of visualized stress clouds for steel bars and concrete are generated (different colors can quickly and intuitively determine the degree of damage to structural components). The numerical model of the developed RC structure was calculated, and a three-dimensional stress cloud was generated considering the damage to the concrete and steel bars in various macroscopic intensity zones, as reported in Figs. 25 and 26.

Under the influence of various seismic IMs, the stress on the concrete and steel bars gradually increases. In zone VI, the maximum stress in the concrete reached 3.767 MPa, and the maximum stress in the steel bars reached 62.99 MPa, indicating relatively mild damage. Although the seismic intensity increases in zones VII and VIII, the change in the concrete stress is insignificant. The damage to the bottom reinforcement increases. The damage to the steel bars in zone VIII is significantly greater than that in zone VII. In zone IX, the maximum stresses in the concrete and steel bars reached 5.685 MPa and 111.5 MPa, respectively. The damage to the RC structure further increases. The damage to the bottom layer of the RC structure in this intensity zone is relatively severe. In contrast, the damage to the upper structure is not significant. The reason is that the bottom layer absorbs and consumes some of the energy, ensuring the safety of the upper structure.

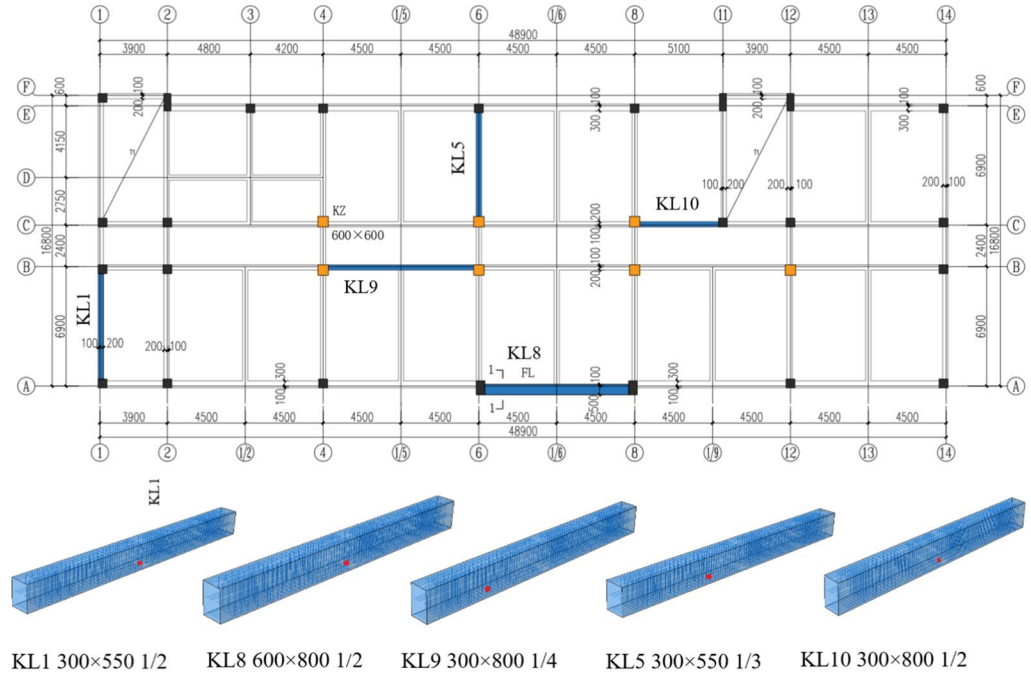

Bottom of beam

(a) Beams/mm

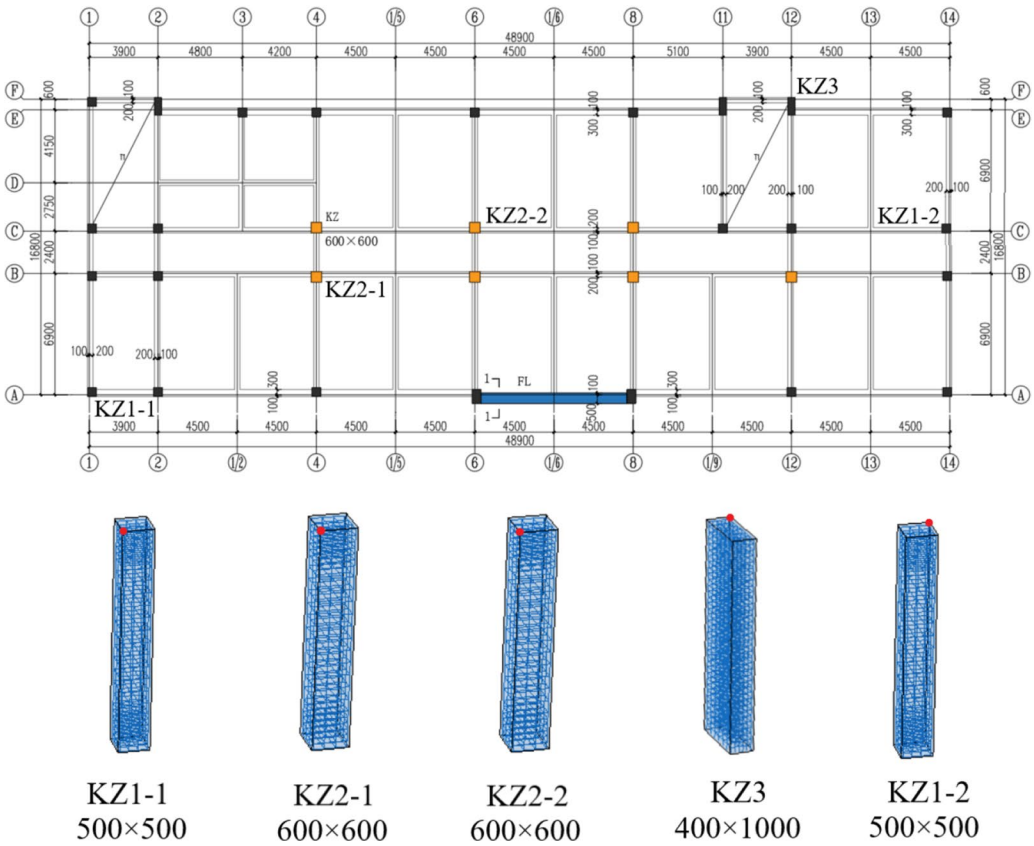

(b) Columns/mm

Fig. 16 The arrangement of selected typical RC frame structure beams and columns

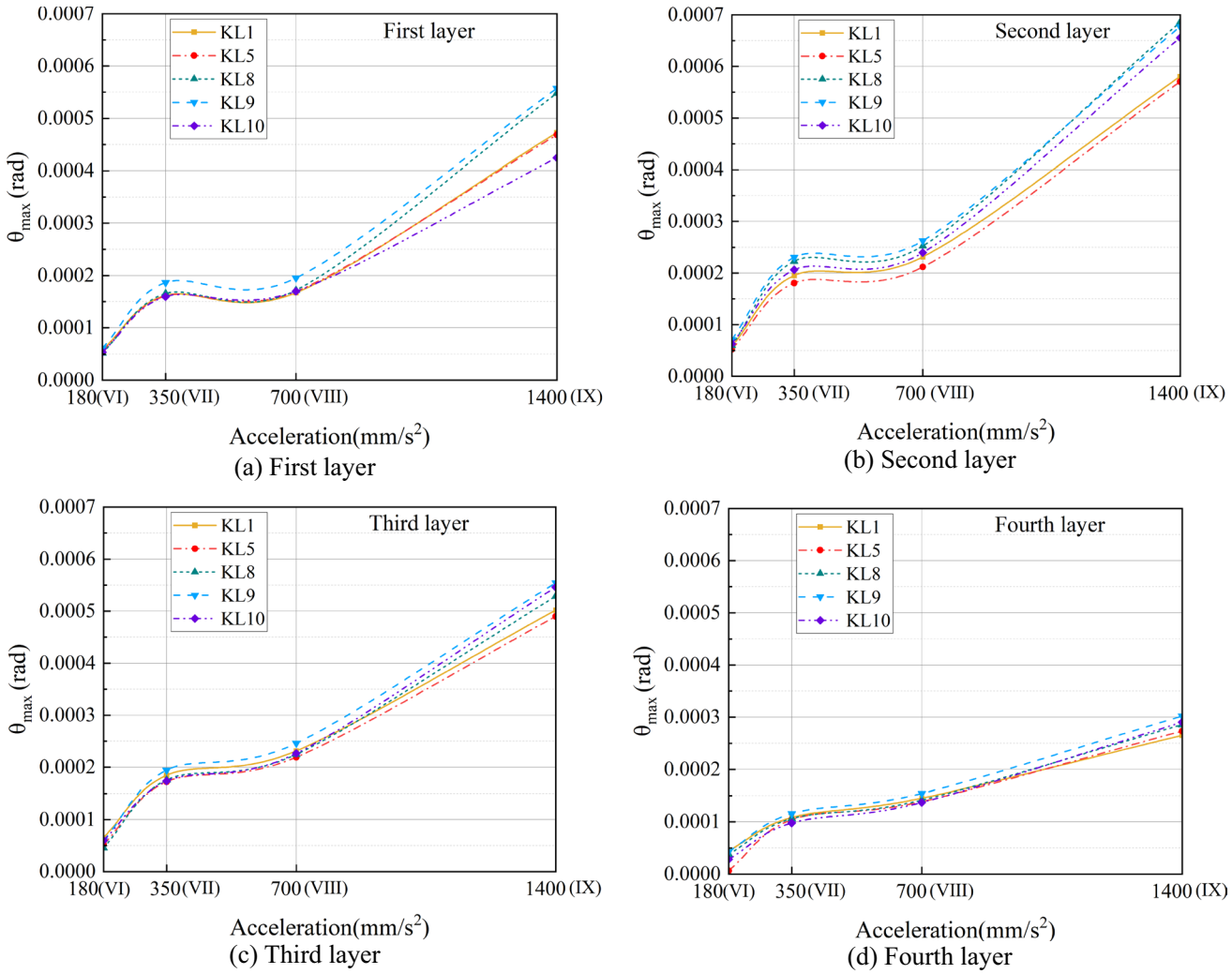

Fig. 17 Damage modal curve of RC structures considering the story drift/θ_{max} (beam)

To compare the empirical and numerical methods, the developed empirical vulnerability matrix and numerical model were calculated and analysed. Empirical and numerical seismic vulnerability comparison curves (ESV and NSV) considering the impact of different seismic IMs were generated, as depicted in Fig. 27. According to the comparison model results, the similarity between the numerical and the empirical curves is high at multiple vulnerability levels. It is worth emphasizing that numerical models have slightly greater prediction accuracy for lower vulnerability levels (DS1, DS2, and DS3) than for higher vulnerability levels (DS4 and DS5). Therefore, the proposed prediction model should be improved and continuously revised considering the characteristics of the site and structure itself. According to the field investigation of actual structures and the established empirical vulnerability model, the failure mode and damage level evaluation of RC structures are highly similar to the simulation analysis results of this numerical model. The damage features of the numerical model are consistent with the general characteristics of earthquake damage in actual RC structures, verifying the rationality of the developed vulnerability model.

Figure 27. Seismic vulnerability comparison curves considering empirical and numerical methods

5 Conclusion

This paper utilizes empirical vulnerability and numerical simulation methods to conduct multidimensional parameter analysis on RC structures. An empirical vulnerability prediction method that considers regional seismic risk models is proposed. A numerical model was established for a four-story RC frame structure in a typical earthquake zone, and the developed model was subjected to multiparameter identification and damage modal analysis using real

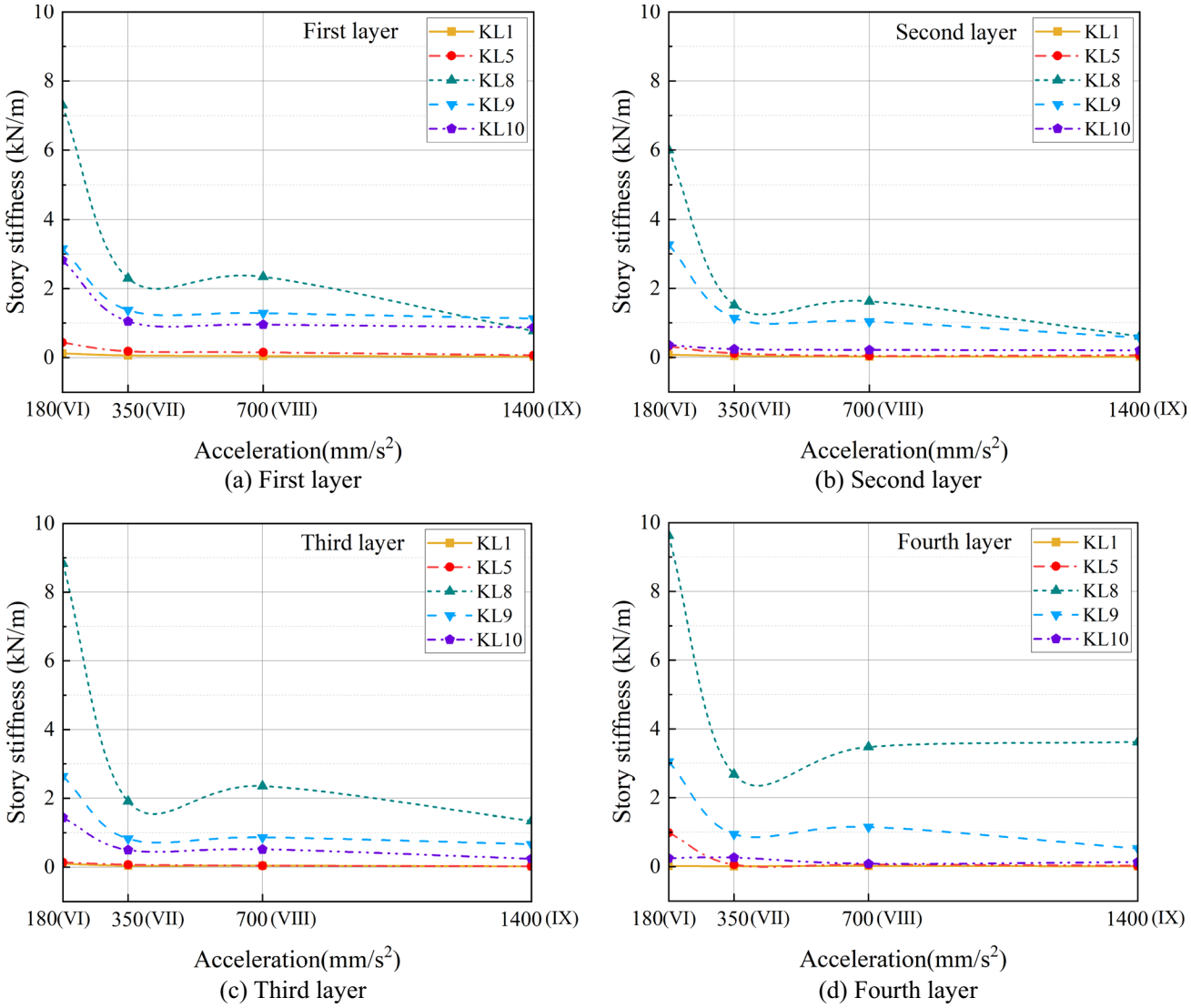

Fig. 18 Damage modal curve of RC structures considering the interlayer stiffness (beam)

accelerations obtained from monitoring at Chinese seismic stations. The following key conclusions were obtained.

1. Using the latest version of China's macroseismic intensity standard, the vulnerability level of the overall RC structure in Dujiangyan city during the 2008 Wenchuan earthquake was assessed, and an empirical vulnerability matrix based on 858 RC structures was established. A nonlinear vulnerability quantification model was proposed to predict the seismic risk of typical RC structures, and its rationality was verified using an innovative structural seismic damage database. The results indicate that the proposed regression model has excellent goodness of fit (all between 0.6 and 1).

2. A three-dimensional finite element model was established for a four-story RC frame structure in a typical earthquake zone. The developed model was subjected to seismic response simulation analysis using 117,863 real seismic acceleration data points from the Wenchuan earthquake. The damage to the structure in zone IX was found to be significantly more severe than that in zones VII and VIII. The structural damage in zone VI is relatively mild. The story drift reached 0.000518 in zone IX, indicating that the RC structure has a certain level of seismic resilience.

3. The real seismic acceleration data of the Wenchuan earthquake were processed and amplitude modulated, and dynamic time history analysis was conducted for layers

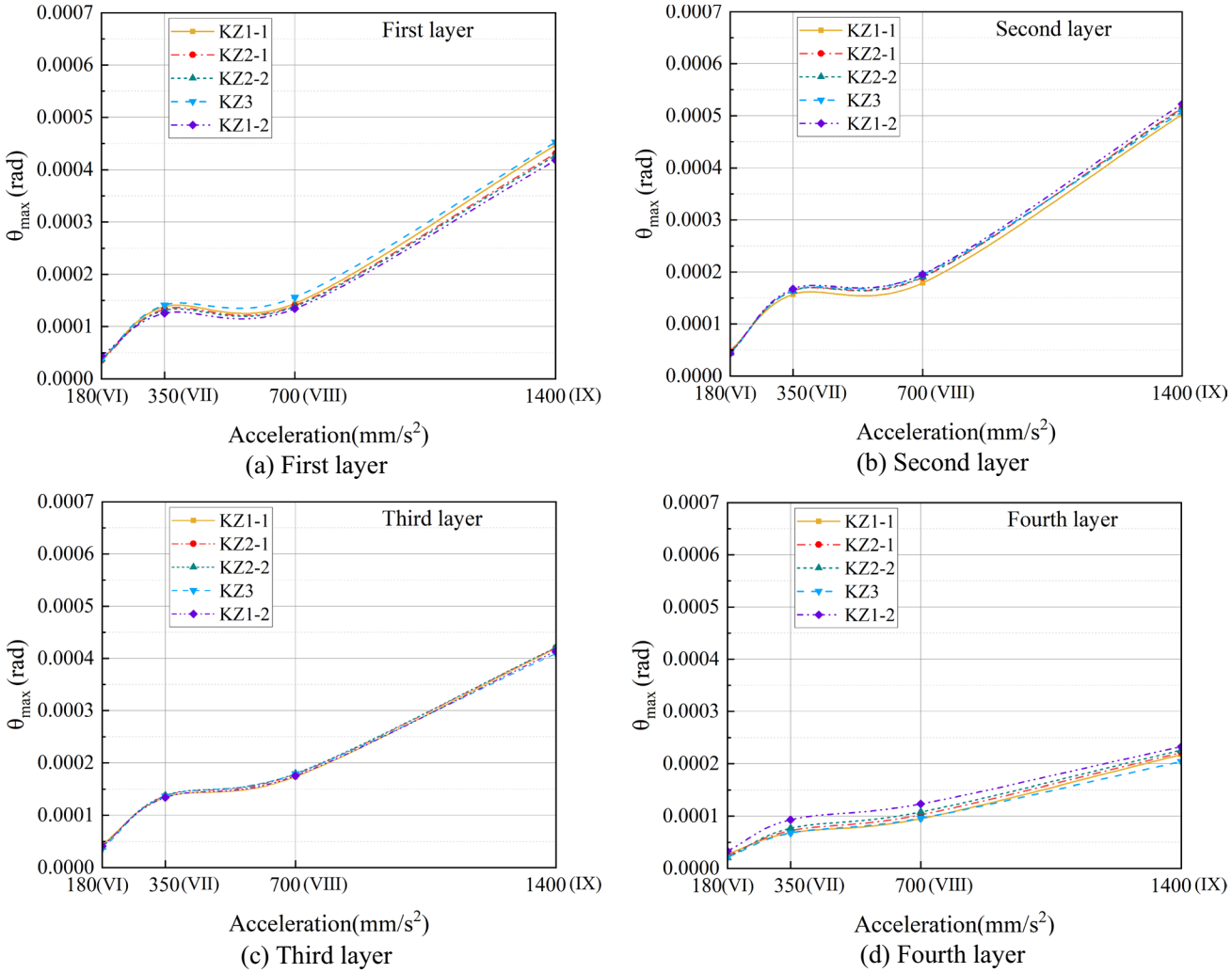

Fig. 19 Damage modal curve of RC structures considering the story drift/θ_{max} (column)

1 to 4 under the influence of different IMs. Time history comparison curves for layers 1 to 4 in multiple intensity zones were generated. The analysis results indicate that the dynamic features of the lower intensity zone do not significantly change, and the structural response and damage further increase with increasing strength.

4. Using the basic theory of incremental dynamic analysis, the story drift and interlayer stiffness of RC structures were determined as engineering requirement parameters. The damage modes of the structure under different IMs were calculated and analysed, and damage mode curves were generated.

5. The impacts of different IMs were considered, the damage features of steel and concrete materials in the established structural finite element model were analysed, and damage stress cloud models of steel and concrete were generated. According to the analysis of the corresponding stress distribution patterns, the effect of lower IMs on structural damage changes is not significant. Therefore, under the influence of higher IMs, the damage to the bottom structure is significantly greater than that to the upper floors.

This paper develops a nonlinear model that can be used to estimate and predict the empirical vulnerability of RC structures. Using numerical simulation methods, multiparameter identification and damage analysis were conducted on the established three-dimensional RC structure model, verifying the rationality of the empirical vulnerability model. This study innovatively provides a hybrid quantitative method of empirical and numerical simulation, which can contribute positively

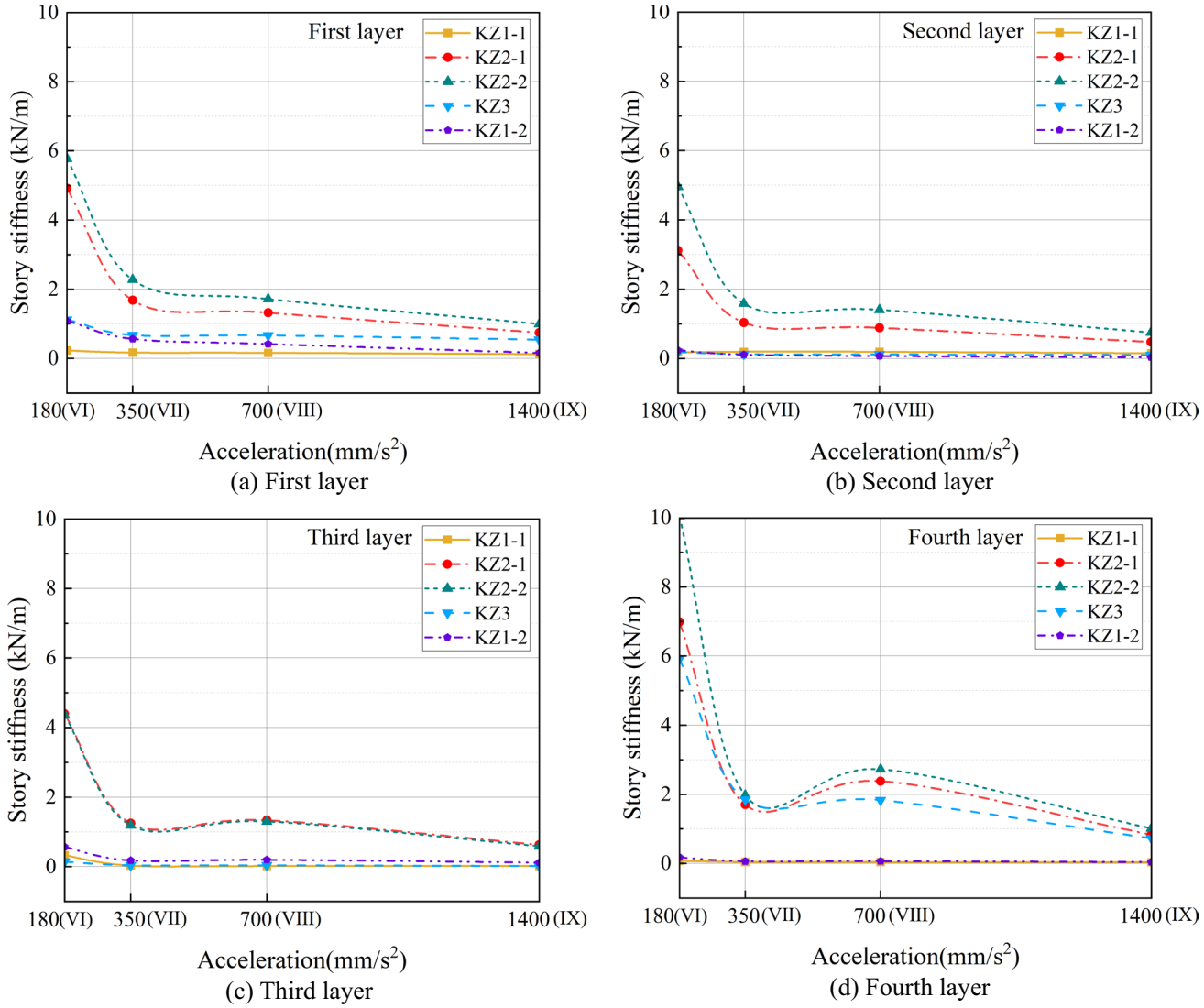

Fig. 20 Damage modal curve of RC structures considering the interlayer stiffness (column)

to evaluating the seismic risk and vulnerability of RC structures. The seismic vulnerability prediction model for RC structures proposed in this paper is influenced by specific seismic data (Wenchuan, 2008) and by site and structural characteristics. Admittedly, the development of empirical vulnerability models relies on field survey data of actual structures. However, the structural damage caused by earthquakes of different intensities has potential uncertainty. The numerical simulation methods are affected by the site conditions, structural characteristics, and seismic sequence in different regions, which limits the generalizability of the numerical models. To make the developed model generalizable, it is necessary to consider adding RC structural damage samples from multiple earthquakes for model updating and further consider the impact of various site and structural characteristics on the model. In earthquake-prone areas, the developed numerical model can be improved considering the material characteristics of the RC structure, site category, and seismic design level of the area. Using the predicted results of the developed model, necessary strengthening measures are proposed for RC structures with severe damage to improve their seismic and resilience capabilities.

Acknowledgements Structural damage sample data were derived from the earthquake field inspection database of the Institute of Engineering

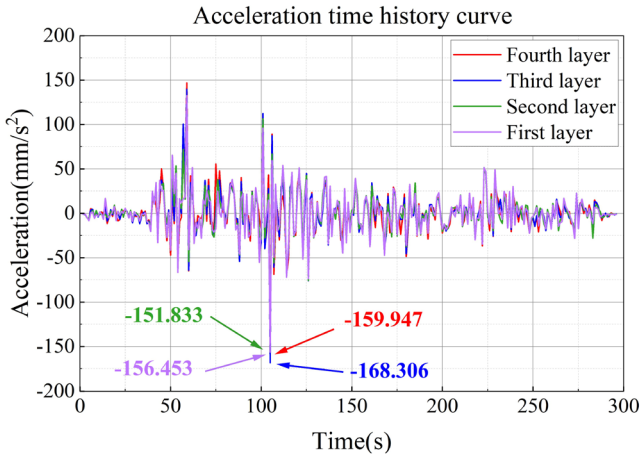

(a) KZ1-1

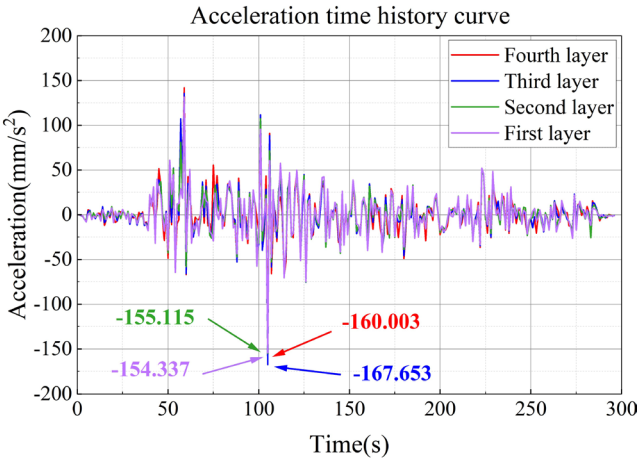

(b) KZ1-2

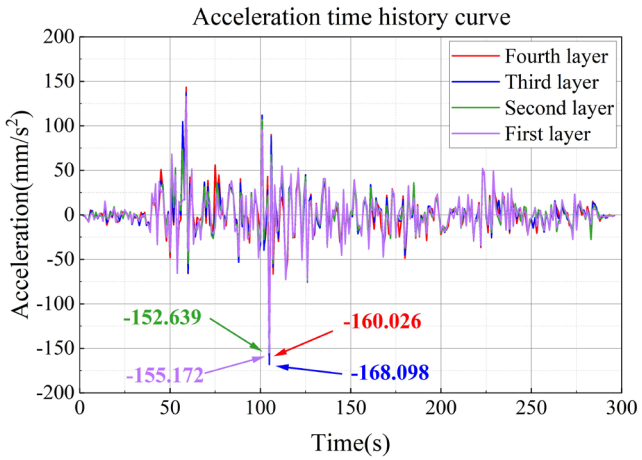

(c) KZ2-1

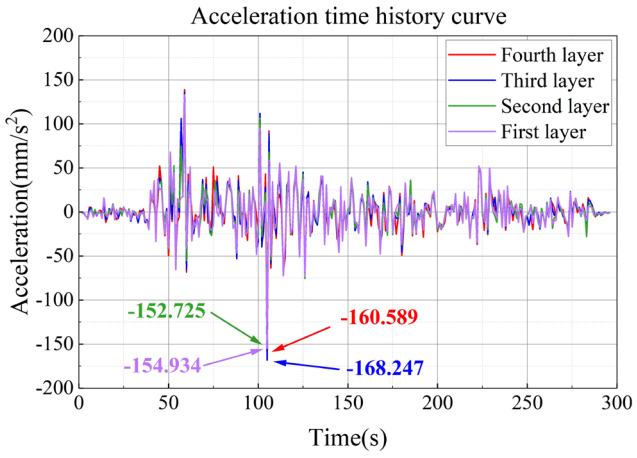

(d) KZ2-2

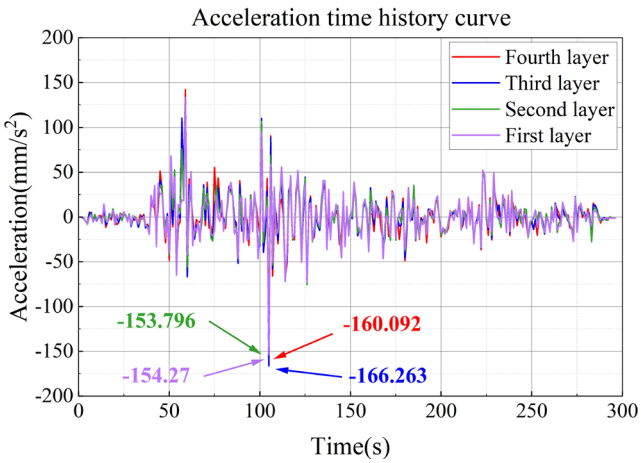

(e) KZ3

Fig. 21 Dynamic time history curves of each floor under the influence of different intensity measures (VI zone)

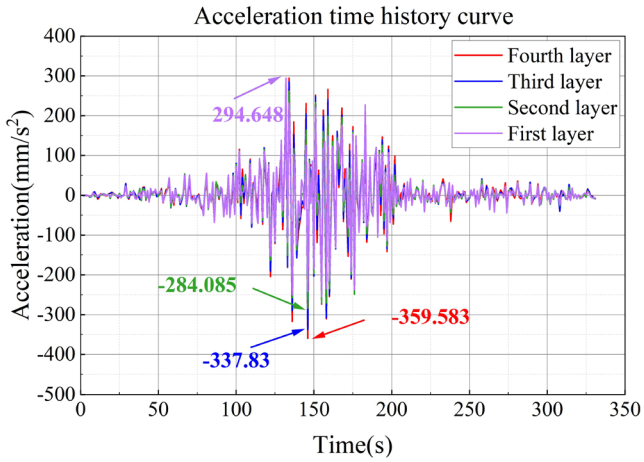

(a) KZ1-1

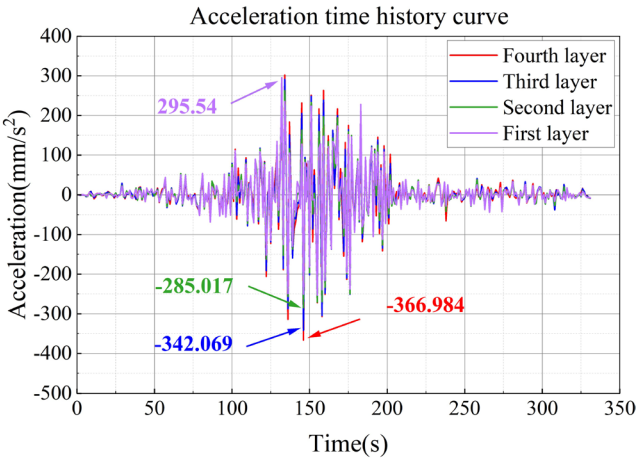

(b) KZ1-2

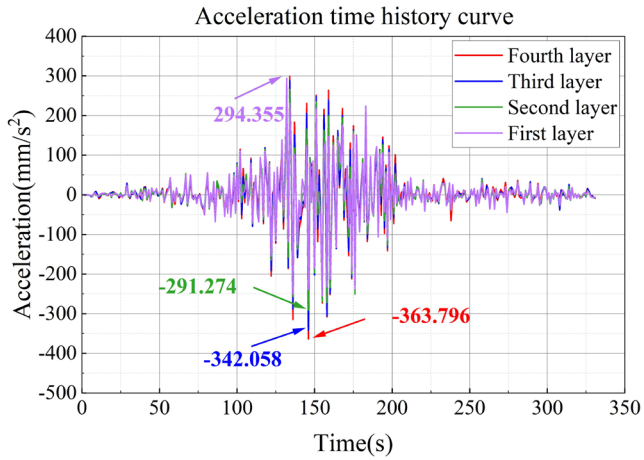

(c) KZ2-1

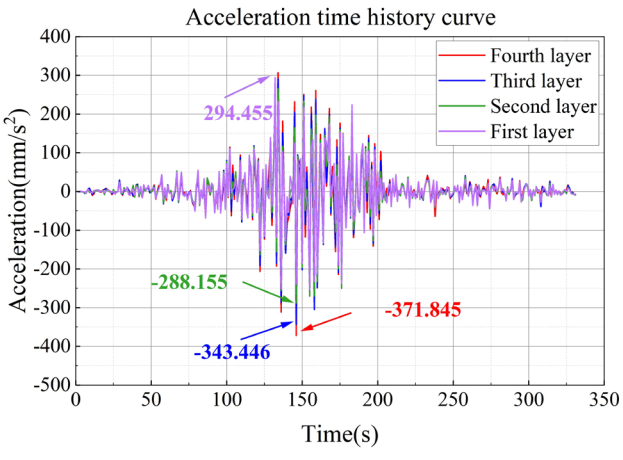

(d) KZ2-2

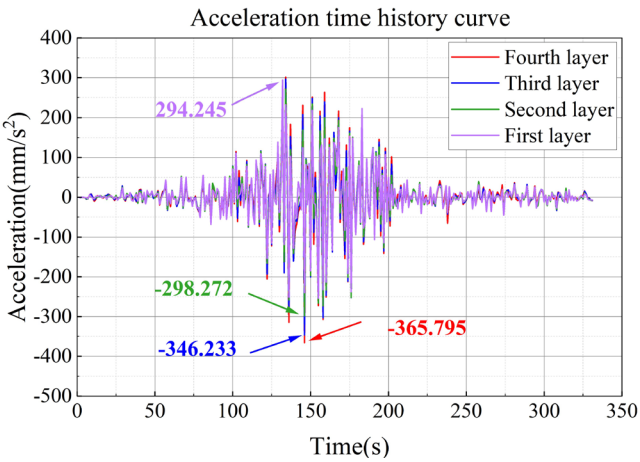

(e) KZ3

Fig. 22 Dynamic time history curves of each floor under the influence of different intensity measures (VII zone)

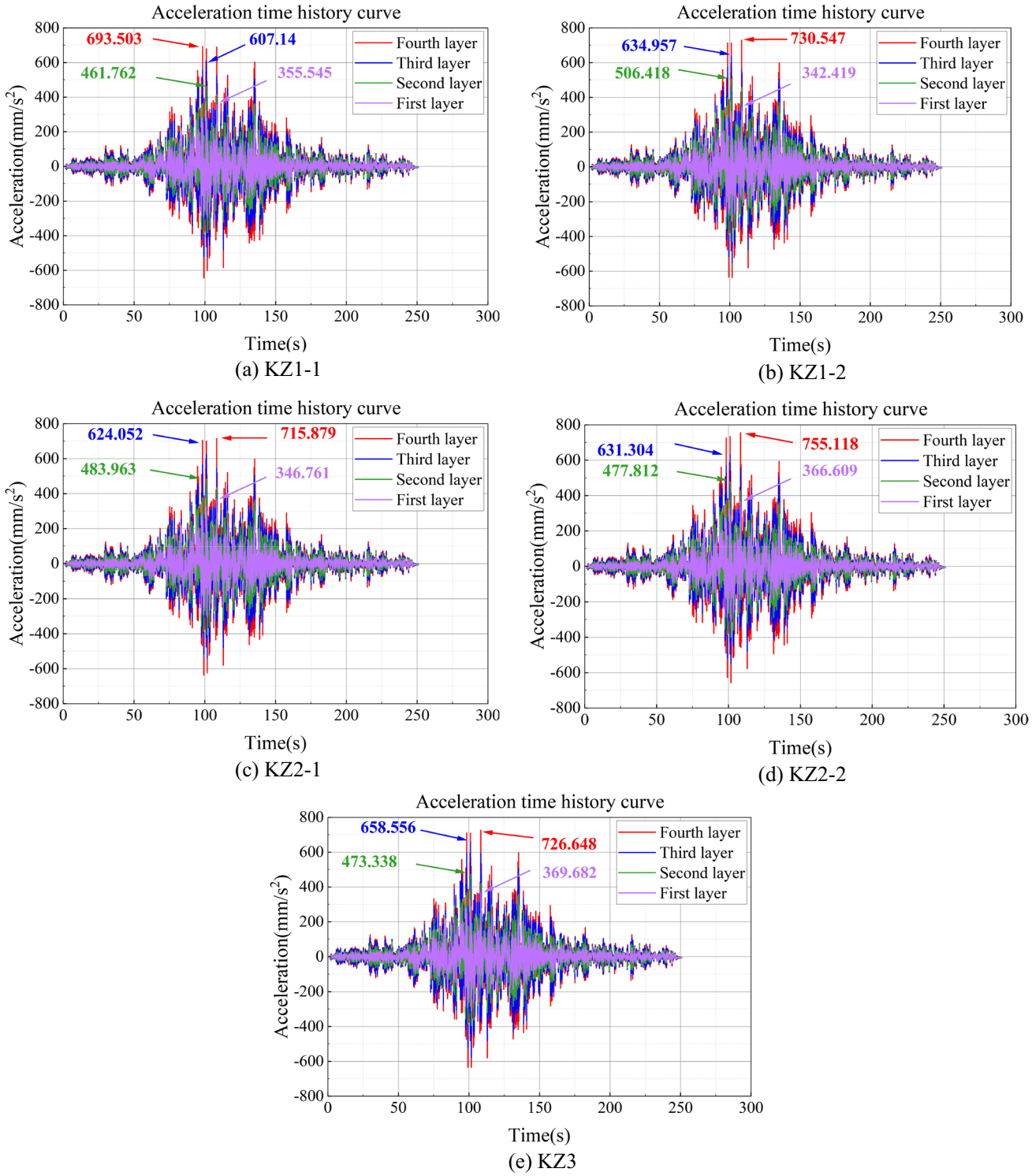

Fig. 23 Dynamic time history curves of each floor under the influence of different intensity measures (VIII zone)

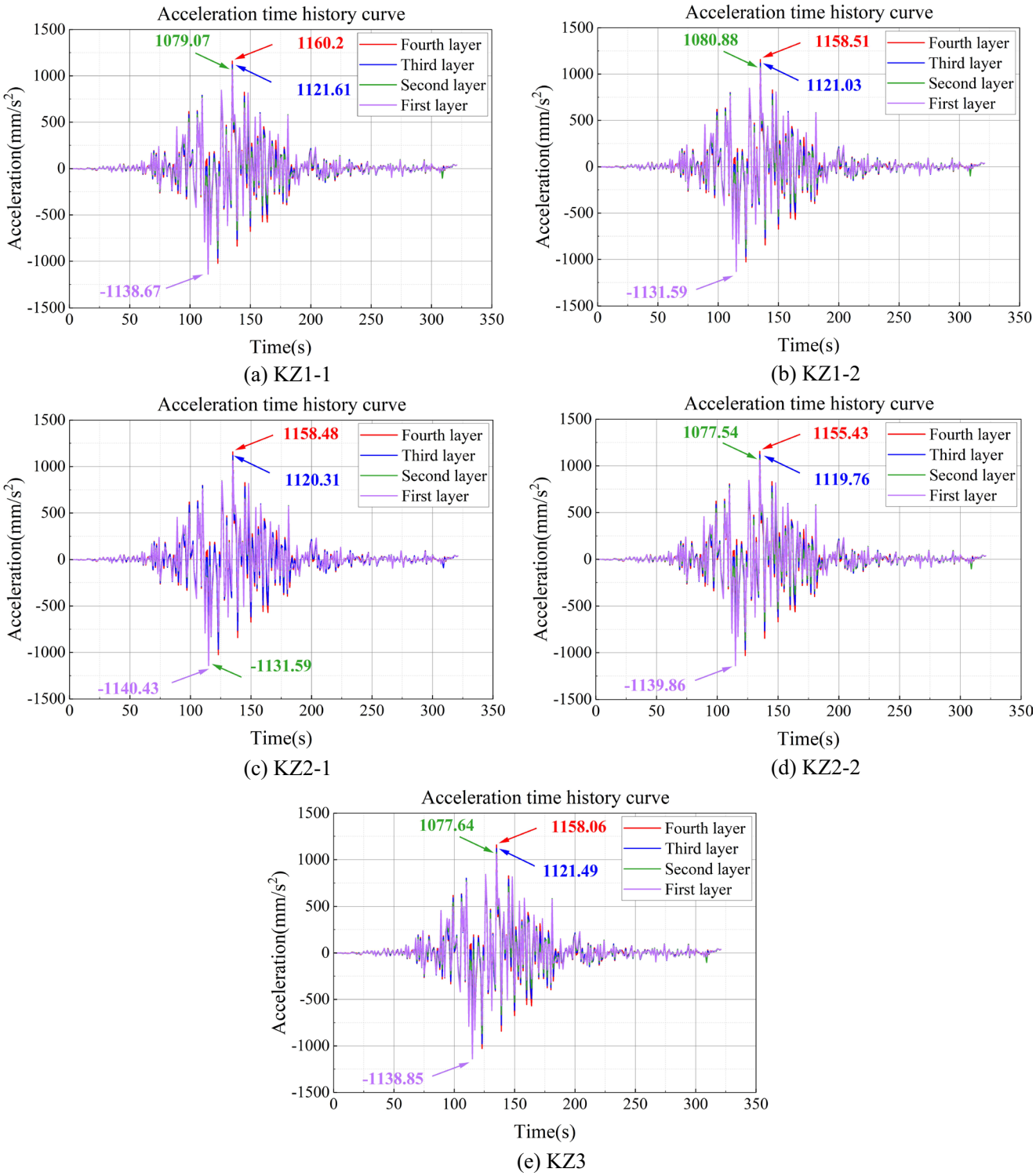

Fig. 24 Dynamic time history curves of each floor under the influence of different intensity measures (IX zone)

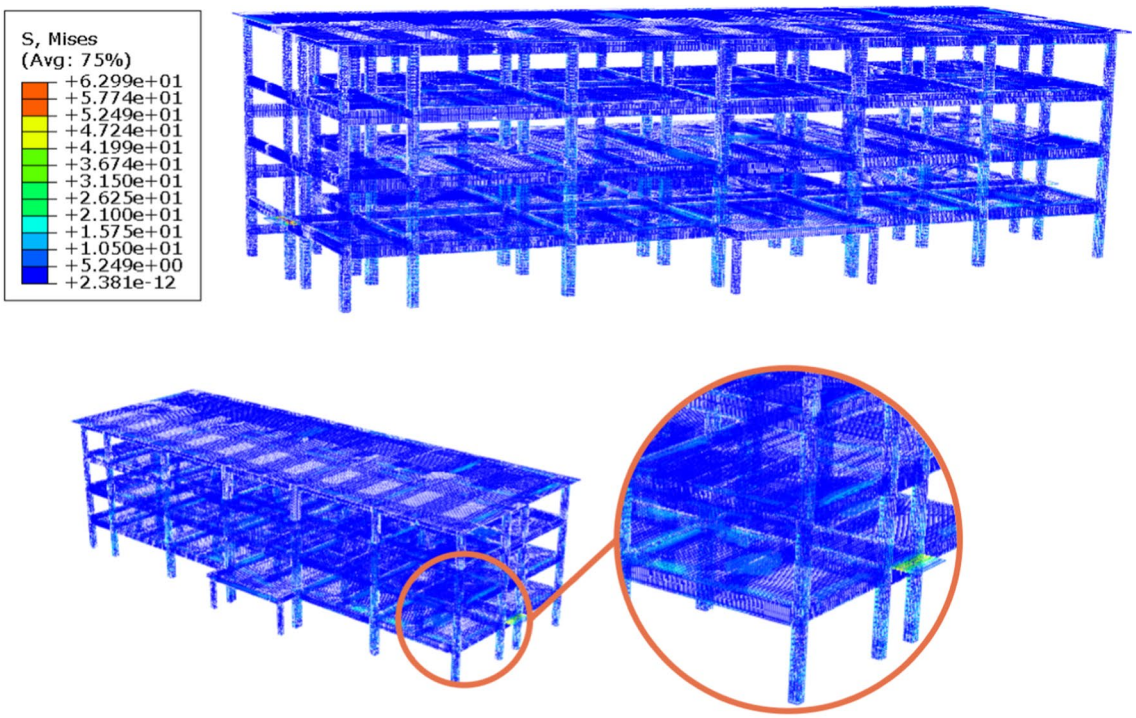

(a) Zone VI

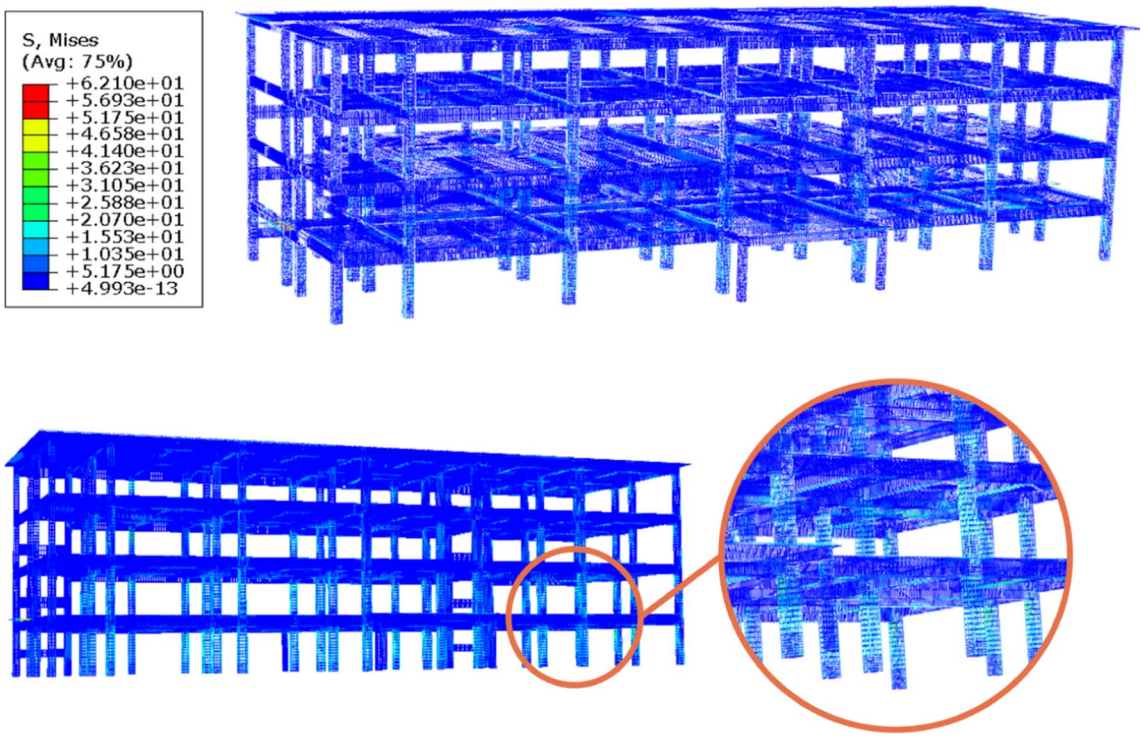

(b) Zone Ⅶ

Fig. 25 Reinforcement stress moire of an RC structure in different intensity zones

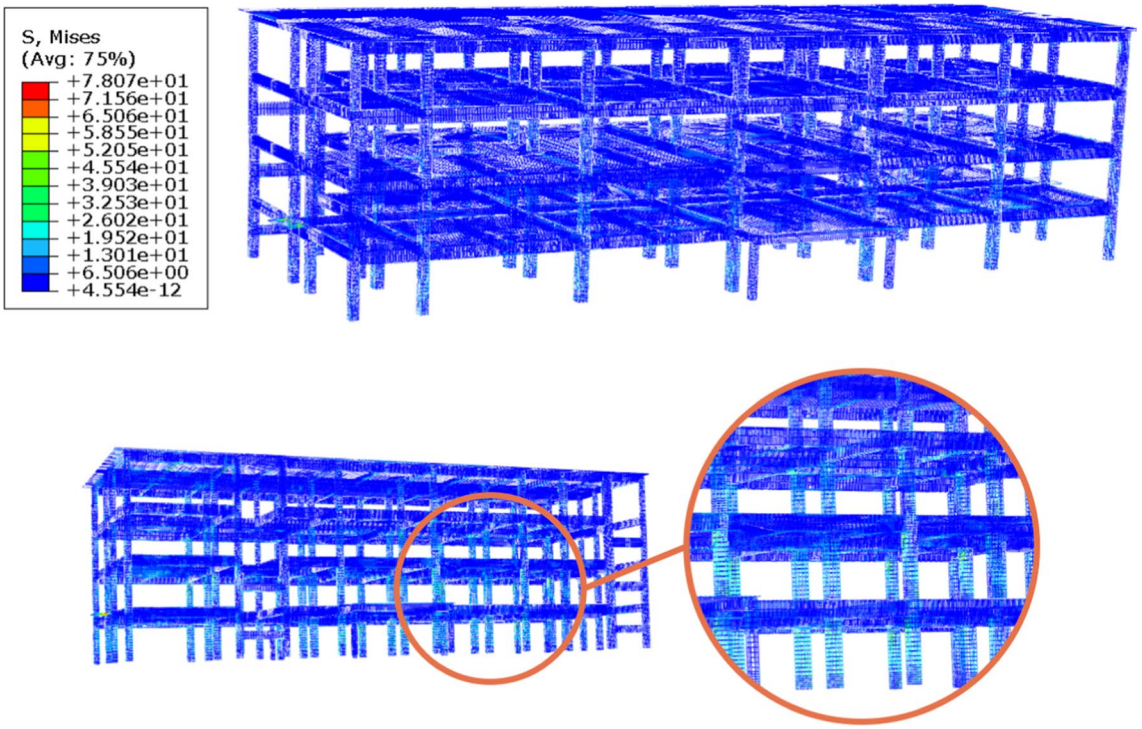

(c) Zone Ⅷ

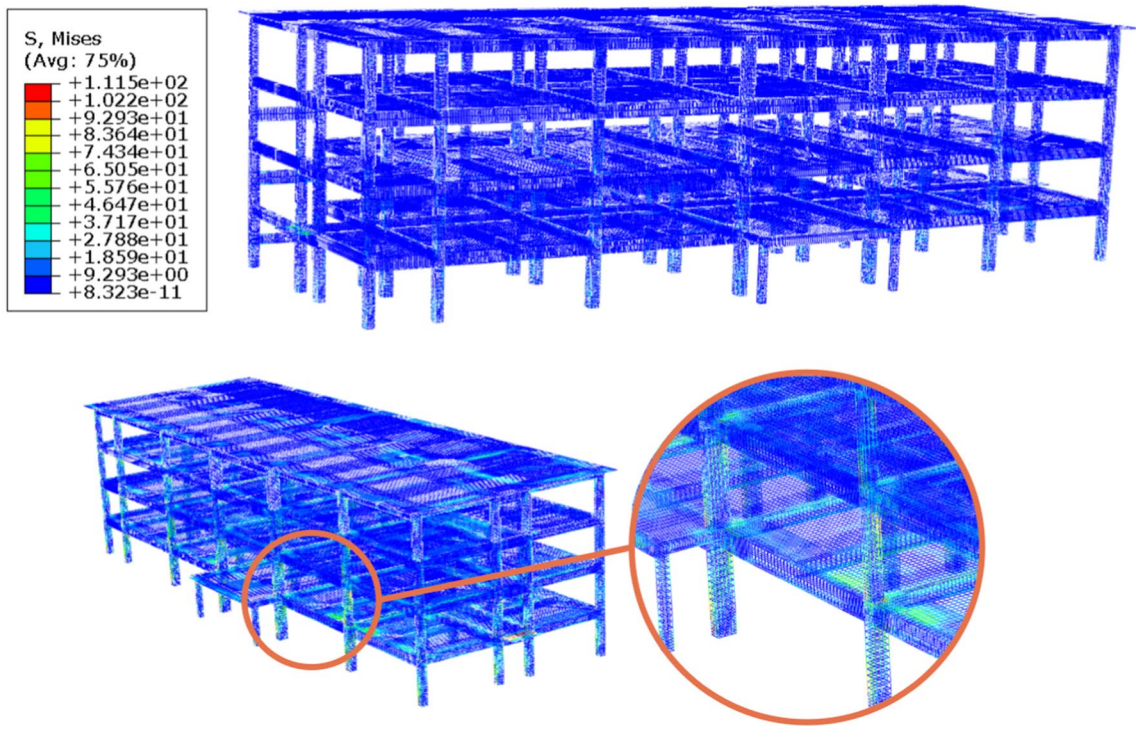

(d) Zone Ⅸ

Fig. 25 (continued)

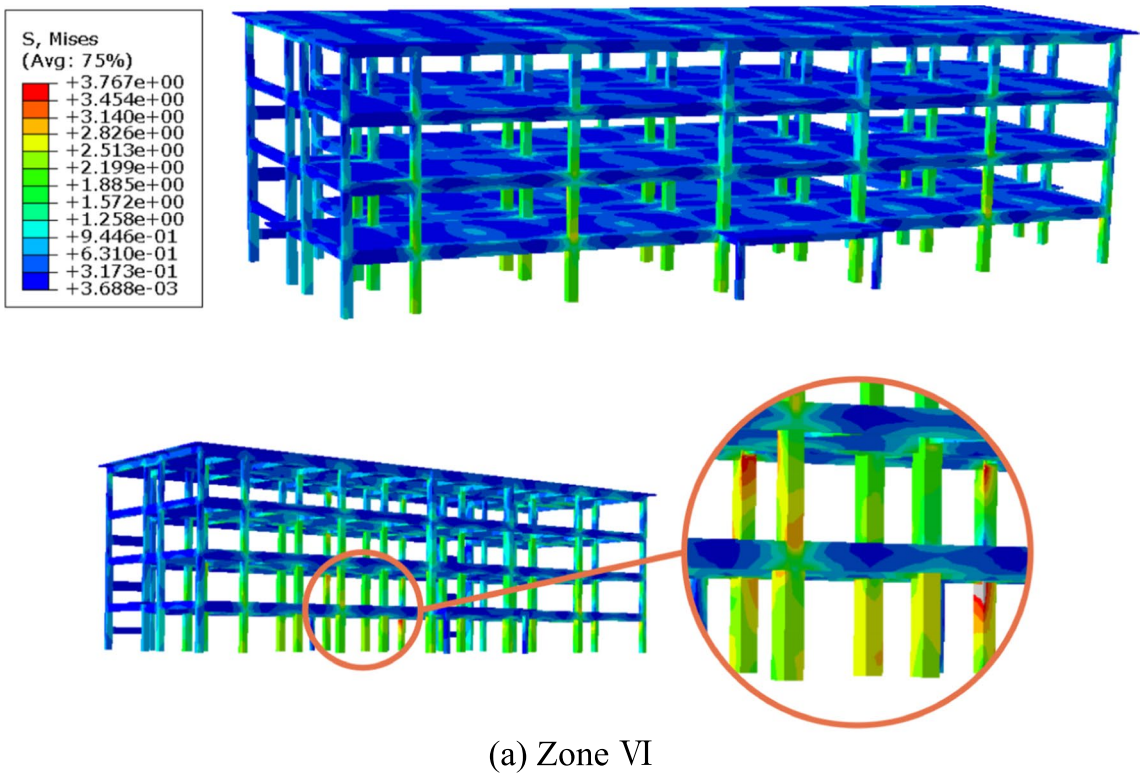

(a) Zone Ⅵ

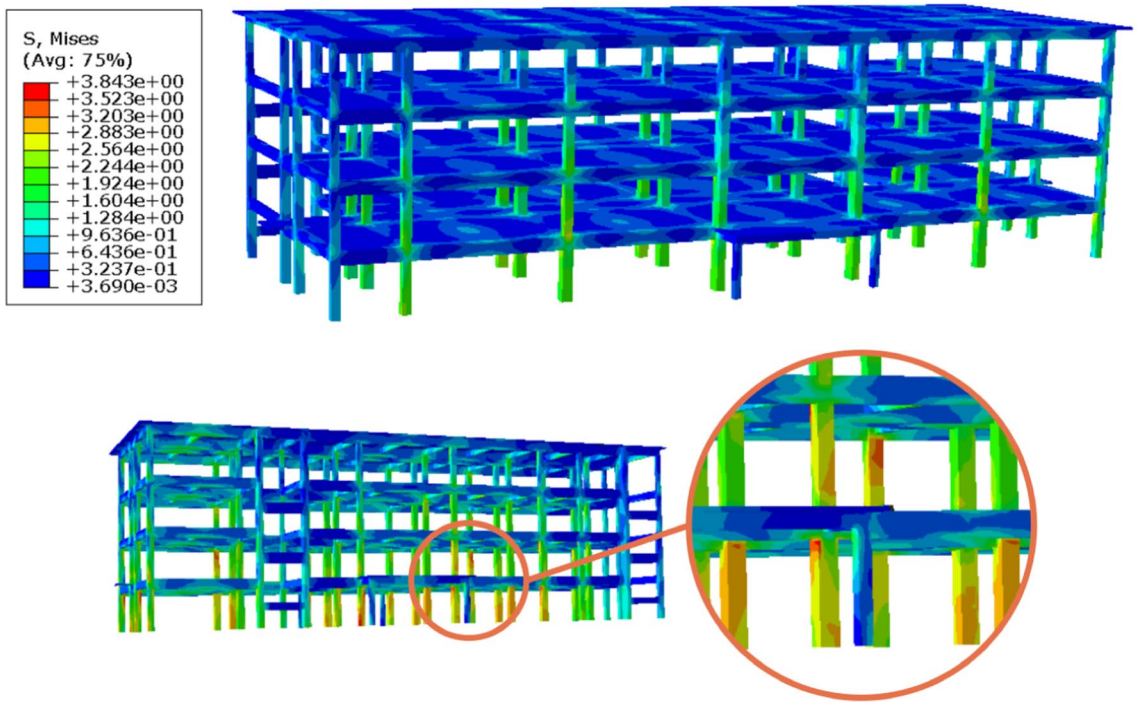

(b) Zone Ⅶ

Fig. 26 Concrete stress moire of an RC structure in different intensity zones

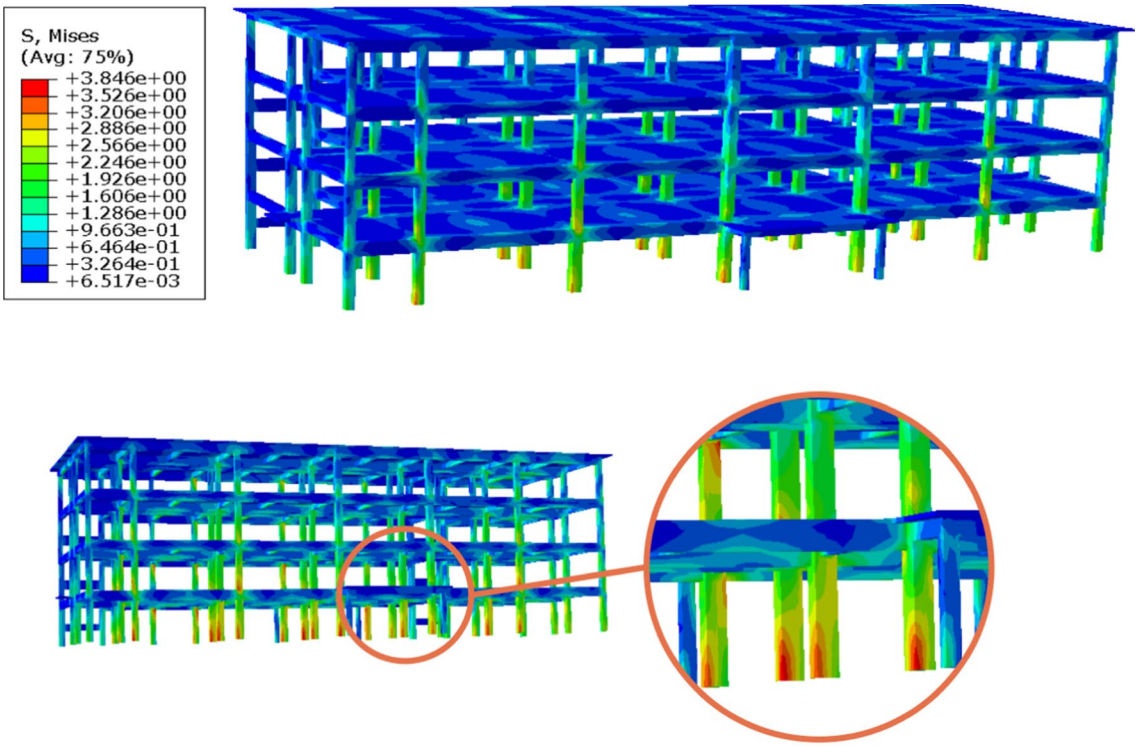

(c) Zone Ⅷ

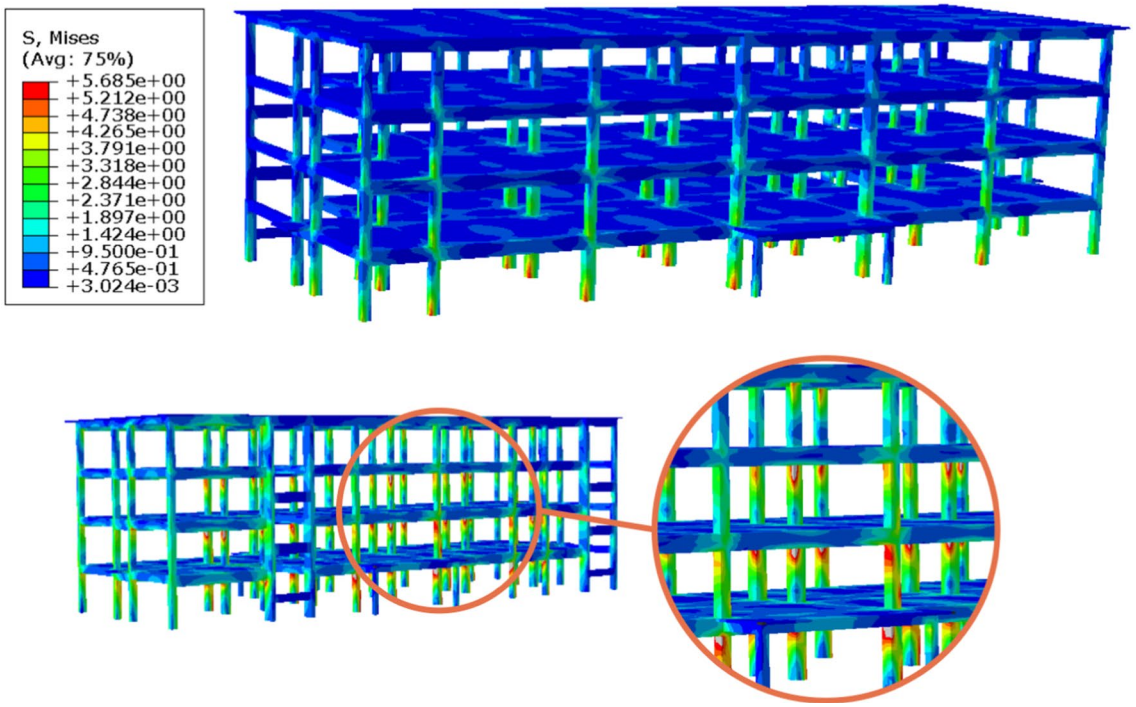

(d) Zone Ⅸ

Fig. 26 (continued)

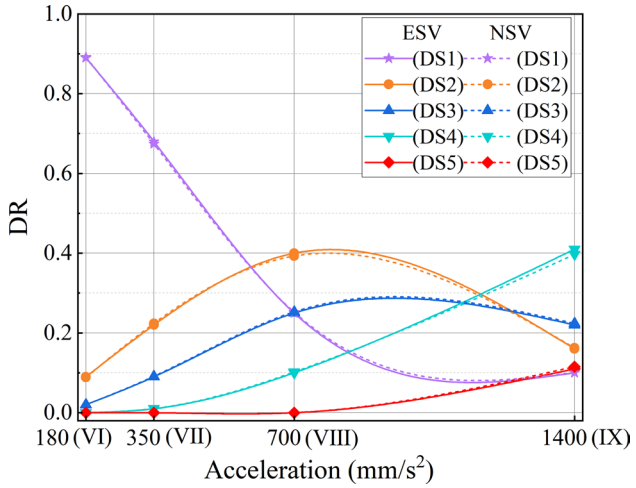

Fig. 27 Seismic vulnerability comparison curves considering empirical and numerical methods

Mechanics (IEM) of the China Earthquake Administration (CEA). Data for this study are provided by the Strong Motion Observation Center, IEM, CEA. We would like to express my sincere gratitude to IEM.

Funding The research described in this paper was financially supported by the Basic Scientific Research Business Expenses of Provincial Universities in Heilongjiang Province (2022-KYYWF-1056), the Scientific Research Fund of Institute of Engineering Mechanics, China Earthquake Administration (Grant No. 2023D39) and a project funded by Heilongjiang Postdoctoral Science Foundation (LBH-Z22294), China.

Data availability Some or all data, models, or code that support the findings of this study are available from the corresponding author upon reasonable request.

Declarations

Conflict of interest The authors declare no conflict of interest, ethics, or otherwise. Confirm informed consent.

Ethical approval It is stated that the study was performed based on ethical standards.

References

1. Hu YX. Earthquake Engineering. Beijing: Earthquake Press; 2006.
2. Li SQ, Gardoni P. Empirical seismic vulnerability models for building clusters considering hybrid intensity measures. J Build Eng. 2023;68:106130. https://doi.org/10.1016/j.jobe.2023.106130.
3. Bigdeli A, Emamikoupaei A, Tsavdaridis KD. Probabilistic seismic demand model and optimal intensity measures for mid-rise steel modular building systems (MBS) under near-field ground motions. J Build Eng. 2023;67:105916. https://doi.org/10.1016/j.jobe.2023.105916.
4. Kim T, Park JH, Yu E. Seismic fragility of low-rise piloti buildings based on 2017 Pohang earthquake damage. J Build Eng. 2023;76:107032. https://doi.org/10.1016/j.jobe.2023.107032.
5. Tekeste GG, Correia AA, Costa AG. Bayesian updating of seismic fragility curves through experimental tests. Bull Earthq Eng. 2023;21:1943–76. https://doi.org/10.1007/s10518-022-01589-4.
6. Boakye J, Murphy C, Gardoni P, Kumar R. Which consequences matter in risk analysis and disaster assessment? Int J Disaster Risk Red. 2022;71:102740. https://doi.org/10.1016/j.ijdrr.2021.102740.
7. Saed G, Balomenos GP. Fragility framework for corroded steel moment-resisting frame buildings subjected to mainshock-aftershock sequences. Soil Dyn Earthq Eng. 2023;171:107975. https://doi.org/10.1016/j.soildyn.2023.107975.
8. Iervolino I. Asymptotic behavior of seismic hazard curves. Struct Saf. 2022;99:102264. https://doi.org/10.1016/j.strusafe.2022.102264.
9. Iervolino I. Implications of GMPE's structure for multi-site seismic hazard. Soil Dyn Earthq Eng. 2023;172:108022. https://doi.org/10.1016/j.soildyn.2023.108022.
10. Iervolino I, Baraschino R, Belleri A, Cardone D, Corte GD, Franchin P, Lagomarsino S, Magliulo G, Marchi A, Penna A, Viggiani LRS, Zona A. Seismic fragility of Italian code-conforming buildings by multi-stripe dynamic analysis of three-dimensional structural models. J Earthq Eng. 2023. https://doi.org/10.1080/13632469.2023.2167889.
11. Tabandeh A, Sharma N, Gardoni P. Seismic risk and resilience analysis of networked industrial facilities. Bull Earthq Eng. 2023. https://doi.org/10.1007/s10518-023-01728-5.
12. Blasi G, Perrone D, Aiello MA. Fragility curves for reinforced concrete frames with retrofitted masonry infills. J Build Eng. 2023. https://doi.org/10.1016/j.jobe.2023.106951.
13. Sharma M, Singh Y, Burton HV. Parametric study on the collapse probability of modern reinforced concrete frames with infills. Earthq Spectra. 2023. https://doi.org/10.1177/87552930231156462.
14. Kazemi F, Asgarkhani N, Jankowski R. Machine learning-based seismic fragility and seismic vulnerability assessment of reinforced concrete structures. Soil Dyn Earthq Eng. 2023;166:107761. https://doi.org/10.1016/j.soildyn.2023.107761.
15. Kazemi F, Asgarkhani N, Jankowski R. Machine learning-based seismic response and performance assessment of reinforced concrete buildings. Arch Civil Mech Eng. 2023;23:94. https://doi.org/10.1007/s43452-023-00631-9.
16. Georgiou A, Kotakis S, Loukidis D, Ioannou I. Case study of seismic assessment of a short irregular historic reinforced concrete structure: time-history vs. pushover nonlinear methods. J Earthq Eng. 2023. https://doi.org/10.1080/13632469.2023.2193652.
17. Zhang H, Cheng X, Li Y, He D, Du X. Rapid seismic damage state assessment of RC frames using machine learning methods. J Build Eng. 2023;65:105797. https://doi.org/10.1016/j.jobe.2022.105797.
18. Elyasi N, Kim E, Yeum CM. A machine-learning-based seismic Vulnerability assessment approach for low-rise RC buildings. J Earthq Eng. 2023. https://doi.org/10.1080/13632469.2023.2220033.
19. Bai Z, Liu T, Zou D, Zhang M, Zhou A, Li Y. Image-based reinforced concrete component mechanical damage recognition and structural safety rapid assessment using deep learning with frequency information. Autom Constr. 2023;150:104839. https://doi.org/10.1016/j.autcon.2023.104839.
20. Li SQ. A simplified prediction model of structural seismic vulnerability considering a multivariate fuzzy membership algorithm. J Earthq Eng. 2023. https://doi.org/10.1080/13632469.2023.2217945.
21. Nale M, Benvenuti E, Chiozzi A, Minghini F, Tralli A. Effect of uncertainties on seismic fragility for out-of-plane collapse

of unreinforced masonry walls. J Build Eng. 2023;75:106936. https://doi.org/10.1016/j.jobe.2023.106936.
22. Del Mese S, Graziani L, Meroni F, Pessina V, Tertulliani A. Considerations on using MCS and EMS-98 macroseismic scales for the intensity assessment of contemporary Italian earthquakes. Bull Earthq Eng. 2023. https://doi.org/10.1007/s10518-023-01703-0.
23. Xofi M, Ferreira TM, Domingues JC, Santos PP, Pereira S, Oliveira C, Reis E, Zezere JL, Garcia RAC, Lourenco PB. On the seismic vulnerability assessment of urban areas using census data: the lisbon metropolitan area as a pilot study area. J Earthq Eng. 2023. https://doi.org/10.1080/13632469.2023.2197078.
24. Gioiella L, Morici M, Dall'Asta, A. Empirical predictive model for seismic damage and economic losses of Italian school building heritage. Int J Disaster Risk Red. 2023. https://doi.org/10.1016/j.ijdrr.2023.103631.
25. Jara JM, Florio E, Olmos BA, Martínez G. Factors influencing soft-story building failures during the September 19, 2017 earthquake in Mexico. Bull Earthq Eng. 2023. https://doi.org/10.1007/s10518-023-01701-2.
26. Sathurshan M, Thamboo J, Mallikarachchi C, Wijesundara K, Dias P. Rapid seismic visual screen method for masonry infilled reinforced concrete framed buildings: Application to typical Sri Lankan school buildings. Int J Disaster Risk Red. 2023. https://doi.org/10.1016/j.ijdrr.2023.103738.
27. Ko YY, Tsai CC, Hwang JH, Hwang YW, Ge L, Chu MC. Failure of engineering structures and associated geotechnical problems during the 2022 ML 6.8 Chihshang earthquake. Bull Earthq Eng. 2023. https://doi.org/10.1007/s11069-023-05993-0.
28. Li SQ. Comparison of RC girder bridge and building vulnerability considering empirical seismic damage. Ain Shams Eng J. 2023. https://doi.org/10.1016/j.asej.2023.102287.
29. Li SQ, Formisano A. Statistical model analysis of typical bridges considering the actual seismic damage observation database. Arch Civil Mech Eng. 2023;23:178. https://doi.org/10.1007/s43452-023-00720-9.
30. Ludovico MD, Cattari S, Verderame G, Vecchio CD, Ottonelli D, Del Gaudio C, Prota A, Lagomarsino S. Fragility curves of Italian school buildings: derivation from L'Aquila 2009 earthquake damage via observational and heuristic approaches. Bull Earthq Eng. 2022. https://doi.org/10.1007/s10518-022-01535-4.
31. Del Gaudio C, Martino GD, Ludovico MD, Manfredi G, Prota A, Ricci P, Verderame GM. Empirical fragility curves from damage data on RC buildings after the 2009 L'Aquila earthquake. Bull Earthq Eng. 2017;15:1425–50. https://doi.org/10.1007/s10518-016-0026-1.
32. Sagbas G, Garjan RS, Sarikaya K, Deniz D. Field reconnaissance on seismic performance and functionality of Turkish industrial facilities affected by the 2023 Kahramanmaras earthquake sequence. Bull Earthq Eng. 2023. https://doi.org/10.1007/s10518-023-01741-8.
33. Khanmohammadi M, Eshraghi M, Sayadi S, Mashhadinezhad MG. Post-earthquake seismic assessment of residential buildings following Sarpol-e Zahab (Iran) earthquake (Mw7.3) part 1: Damage types and damage states. Soil Dyn Earthq Eng. 2023;173:108121. https://doi.org/10.1016/j.soildyn.2023.108121.
34. Khanmohammadi M, Eshraghi M, Sayadi S, Mashhadinezhad MG. Post-earthquake seismic assessment of residential buildings following Sarpol-e Zahab (Iran) earthquake (Mw7.3) part 2: Seismic vulnerability curves using quantitative damage index. Soil Dyn Earthq Eng. 2023;173:108120. https://doi.org/10.1016/j.soildyn.2023.108120.
35. Li SQ, Liu HB, Du K, Han JC, Li YR, Yin LH. Empirical seismic vulnerability probability prediction model of RC structures considering historical field observation. Struct Eng Mech. 2023;86(4):547–71. https://doi.org/10.12989/sem.2023.86.4.547.
36. Li SQ, Chen YS. Vulnerability and economic loss evaluation model of a typical group structure considering empirical field inspection data. Int J Disaster Risk Red. 2023;88:103617. https://doi.org/10.1016/j.ijdrr.2023.103617.
37. Li SQ. Empirical resilience and vulnerability model of regional group structure considering optimized macroseismic intensity measure. Soil Dyn Earthq Eng. 2023;164:107630. https://doi.org/10.1016/j.soildyn.2022.107630.
38. Formisano A, Chieffo N, Asteris PG, Lourenço. Seismic risk scenario for the historical centre of castelpoto in Southern Italy. Earthquake Eng Struct Dynam. 2023. https://doi.org/10.1002/eqe.3887.
39. Kassem MM, Nazri FM, Farsangi EN, Ozturk B. Development of a uniform seismic vulnerability index framework for reinforced concrete building typology. J of Build Eng. 2023;47:103838. https://doi.org/10.1016/j.jobe.2021.103838.
40. Elaissi AM, Argyroudis SA, Kassem MM, Nazri FM. Integrated seismic vulnerability assessment of road network in complex built environment toward more resilient Cities. Sustain Cities Soc. 2023. https://doi.org/10.1016/j.scs.2022.104363.
41. Li SQ, Chen YS, Liu HB, Del Gaudio C. Empirical seismic vulnerability assessment model of typical urban buildings. Bull Earthq Eng. 2023. https://doi.org/10.1007/s10518-022-01585-8.
42. Li SQ, Liu HB. Vulnerability prediction model of typical structures considering empirical seismic damage observation data. Bull Earthq Eng. 2022;20:5161–203. https://doi.org/10.1007/s10518-022-01395-y.
43. GB/T 17742. The Chinese seismic intensity scale. 1999 (in Chinese)
44. GB/T 17742. The Chinese seismic intensity scale. 2008 (in Chinese)
45. GB/T 17742. The Chinese seismic intensity scale. 2020 (in Chinese)
46. Ornthammarath T, Chua CT, Suppasri A, Foytong P. Seismic damage and comparison of fragility functions of public and residential buildings damaged by the 2014 Mae Lao (Northern Thailand) earthquake. Earthq Spectra. 2023;39(1):126–47. https://doi.org/10.1177/87552930221131830.
47. Chieffo N, Clementi F, Formisano A, Lenci S. Comparative fragility methods for seismic assessment of masonry buildings located in Muccia (Italy). J Build Eng. 2019;25:100813. https://doi.org/10.1016/j.jobe.2019.100813.
48. Chieffo N, Mosoarca M, Formisano A, Lourenço PB, Milani G. The effect of ground motion vertical component on the seismic response of historical masonry buildings: the case study of the Banloc Castle in Romania. Eng Struct. 2021;249:113346. https://doi.org/10.1016/j.engstruct.2021.113346.
49. Chieffo N, Formisano A, Landolfo R, Milani G. A vulnerability index based-approach for the historical centre of the city of Latronico (Potenza, Southern Italy). Eng Fail Anal. 2022;136:106207. https://doi.org/10.1016/j.engfailanal.2022.106207.
50. Zucconi M, Ludovico MD, Sorrentino L. Census-based typological usability fragility curves for Italian unreinforced masonry buildings. Bull Earthq Eng. 2022. https://doi.org/10.1007/s10518-022-01361-8.
51. Ruggieri S, Liguori FS, Leggieri V, Bilotta A, Madeo A, Casolo S, Uva G. An archetype-based automated procedure to derive global-local seismic fragility of masonry building aggregates: META-FORMA-XL. Int J Disaster Risk Reduct. 2023;95:103903. https://doi.org/10.1016/j.ijdrr.2023.103903.
52. Ruggieri S, Calò M, Cardellicchio A, Uva G. Analytical-mechanical based framework for seismic overall fragility analysis of existing RC buildings in town compartments. Bull Earthq Eng. 2022;20:8179–216. https://doi.org/10.1007/s10518-022-01516-7.

53. Ruggieri S, Vukobratović V. Acceleration demands in single-storey RC buildings with flexible diaphragms. Eng Struct. 2023;275:115276. https://doi.org/10.1016/j.engstruct.2022.115276.
54. Vukobratović V, Ruggieri S. Floor acceleration demands in a twelve-storey RC shear wall building. Buildings. 2021;11:38. https://doi.org/10.3390/buildings11020038.
55. Formisano A, De Matteis G, Panico S, Calderoni B, Mazzolani FM. Full-scale test on existing RC frame reinforced with slender shear steel plates. Proceedings of the 5th International Conference on Behaviour of Steel Structures in Seismic Areas – Stessa. 2006;2006:827–834.
56. Chieffo N, Formisano A, Miguel Ferreira T. Damage scenario-based approach and retrofitting strategies for seismic risk mitigation: an application to the historical Centre of Sant'Antimo (Italy). Eur J Environ Civ Eng. 2021;25(11):1929–48. https://doi.org/10.1080/19648189.2019.1596164.
57. Mohebi B, Yazdanpanah O, Kazemi F, Formisano A. Seismic damage diagnosis in adjacent steel and RC MRFs considering pounding effects through improved wavelet-based damage-sensitive feature. J Build Eng. 2021;33:101847. https://doi.org/10.1016/j.jobe.2020.101847.
58. Li SQ, Zhong J. Development of a seismic vulnerability and risk model for typical bridges considering innovative intensity measures. Eng Struct. 2024;302:117431. https://doi.org/10.1016/j.engstruct.2023.117431
59. Li SQ. Improved seismic intensity measures and regional structural risk estimation models. Soil Dyn Earthq Eng. 2024;176:108256. https://doi.org/10.1016/j.soildyn.2023.108256
60. Li SQ, Formisano A. Updated empirical vulnerability model considering the seismic damage of typical structures. Bull Earthq Eng 2024;22(3):1147–1185. https://doi.org/10.1007/s10518-023-01814-8
61. Li SQ, Gardoni P. Seismic loss assessment for regional building portfolios considering empirical seismic vulnerability functions. Bull Earthq Eng 2024;22(2):487–517. https://doi.org/10.1007/s10518-023-01793-w
62. Ministry of Housing and Urban-Rural Development of the People's Republic of China. Code for design of concrete structures, China (GB 50010–2020). 2020.